

QUANTUM DOT LASERS

by

Mohammed Eshphaq Hossain (132410)

Muhammad Sami Irfan (132421)

Mehedi Hasan (132423)

A.K.M Salman Hosain (132488)

A Thesis Submitted to the Academic Faculty in Partial Fulfillment of the
Requirements for the Degree of

BACHELOR OF SCIENCE IN ELECTRICAL AND ELECTRONIC ENGINEERING



Department of Electrical and Electronic Engineering
Islamic University of Technology (IUT)
Gazipur, Bangladesh

November 2017

QUANTUM DOT LASERS

Approved by:

Dr. Syed Iftekhar Ali
Supervisor and Associate Professor,
Department of Electrical and Electronic Engineering,
Islamic University of Technology (IUT),
Boardbazar, Gazipur-1704.

Date:

Table of Contents

List of Figures	iv
List of Acronyms	vi
Acknowledgements	vii
Abstract	viii
1 Introduction	1
1.1 INTRODUCTION AND BACKGROUND	ERROR! BOOKMARK NOT DEFINED.
1.2 QUANTUM CONFINEMENT EFFECTS	3
1.3 PRODUCTION METHODS OF QUANTUM DOTS	5
1.3.1 COLLOIDAL SYNTHESIS.....	6
1.3.2 PLASMA SYNTHESIS.....	6
1.3.3 FABRICATION.....	7
1.3.4 VIRAL ASSEMBLY.....	8
1.3.5 ELECTROCHEMICAL ASSEMBLY.....	9
1.3.6 BULK MANUFACTURE.....	9
1.3.7 HEAVY METAL QUANTUM DOTS.....	11
1.4 DEVELOPMENT OF QUANTUM DOT LASERS.....	11
2 Quantum dot applications in laser	13
2.1 INTRODUCTION.....	13
2.2 LASER.....	14
2.2.1 COMPONENTS OF A LASER.....	14
2.2.2 LASING MATERIAL OR ACTIVE MATERIAL.....	15
2.2.3 EXTERNAL ENERGY SOURCE.....	15
2.2.4 OPTICAL RESONATOR.....	15
2.3 WHY QUANTUM DOT IN LASER.....	16
2.4 Q.DOT LASER VS Q.WELL LASER.....	16
2.5 BOTTLENECKS.....	17
2.6 DEVELOPMENTS OF QUANTUM DOT LASERS.....	17
2.7 PREDICTED ADVANTAGES OF QDL.....	18
2.8 DIFFERENT TYPES OF QDL.....	19
2.8.1 HIGH SPEED QDL.....	19
2.8.2 DIRECTLY MODULATED QDL.....	20
2.8.3 MODE LOCKED QDL.....	20
2.8.4 InP BASED QDL.....	21
2.8.5 HIGH POWER QDL.....	22
2.8.6 QDL FOR COOLERLESS PUMP SOURCES.....	23
2.8.7 SINGLE MODE TAPERED LASERS.....	24
2.9 APPLICATIONS OF QDL.....	25
3 Modeling of quantum dot lasers	26
3.1 THE RIDGE WAVEGUIDE QD LASER.....	26
3.1.1 THE RATE EQUATION MODEL.....	27
4 Simulation of RES model	31
4.1 SIMULATION OF RATE EQUATIONS IN MATLAB.....	31
4.2 QD LAYER ELECTRON DENSITY VS TIME.....	31

4.3	QD LAYER HOLE DENSITY VS TIME.....	32
4.4	WETTING LAYER ELECTRON DENSITY VS TIME.....	33
4.5	WETTING LAYER HOLE DENSITY VS TIME.....	34
4.6	ELECTRON DENSITY IN WETTING LAYER IN STEADY STATE.....	36
4.7	HOLE DENSITY IN WL IN STEADY STATE.....	37
5	Conclusion and future work.....	39
5.1	CONCLUSION.....	39
5.2	FUTURE WORK.....	39
	References.....	40

List of Figures

Figure 1.1: Quantum Dot wavelength and size.....	2
Figure 1.2: Semiconductor Quantum dot.....	2
Figure 1.3: – Comparisons of quantum wells, wires, rods and dots.....	3
Figure 1.4: Comparison of the quantization of density of states: (a) bulk, (b) quantum well, (c) quantumwire, (d) quantum dot.....	5
Figure 1.5: Colloidal synthesis.....	6
Figure 1.6: Stranski-Krastanov growth.....	8
Figure 1.7: Viral assembly.....	9
Figure 1.8: The historical evolution of QD lasers from the beginning.....	12
Figure 2.1: Lasing Operation.....	14
Figure 2.2: LASER Using QD Layer.....	18
Figure 2.3: BER measurement of QD laser module at 8 Gb/s and 10 Gb/s (a) and at 10 Gb/s for different temperatures (b), inset shows the corresponding eye patterns.....	20
Figure 2.4: Autocorrelation trace of a passively mode-locked quantumdot laser at 1.3 μm and 80 GHz repetition rate.....	21
Figure 2.5: Small signal modulation response for a QDash DFB laser at four different pulsed (10 μs pulses at a duty cycle of 2%) bias levels.....	22
Figure 2.6: PL spectra of dot layers with different dot sizes resulting in different transition energy splittings between fundamental and first excited state transitions (a=47meV,b= 56 meV, c = 65 meV).....	23
Figure 2.7: Total output power and wall-plug efficiency of a quantum dot high power laser with 1 mm cavity length and 100 μm broad contact stripes.....	24
Figure 2.8: Emission spectra for 3 different temperatures of a single mode emitting QD tapered laser are shown.....	25
Figure 3.1: A) The ridge waveguide QD laser.....	27
Figure 3.1. B) The four energy states of the two-level system.....	27
Figure 4.1: QD electron density vs time.....	31
Figure 4.2: Curves simulated for hole density in QD layer vs time.....	33
Figure 4.3: WL electron density vs time.....	34

Figure 4.4: WL hole density vs time curves.....35
Figure 4.5: Electron density in WL in steady state vs pump current.....36
Figure 4.6: Hole density in WL in steady state vs pump current.....37

List of Acronyms

QD	Quantum Dot
QDL	Quantum Dot Laser
WL	Wetting Layer
RES	Rate Equation System

Acknowledgements

At the very beginning, we are very grateful to almighty Allah for giving us strength and confidence to complete our research.

We would like to thank our supervisor, Dr. Syed Iftekhhar Ali, for his regular guidance, supervision, and constructive suggestions during this research.

Finally we would like to thank our parents, all of our friends and well wishers for their moral support and helpful discussion during this thesis.

Abstract

Semiconductor quantum dots have gained considerable research interest in the recent years. Their unique tunable electrical and optical properties make them ideal for applications in transistors, LEDs, lasers and solar cells. In particular their application in semiconductor laser is an area of research that draws considerable interest. In this work, we review the recent advancements in quantum dot laser technology. A brief review of semiconductor nanostructures and quantum confinement effect is presented at the beginning. Various fabrication methods of quantum dots are discussed as well. Secondly, we examined the physical properties of quantum dot lasers along with history and development of quantum dot laser technology and different kinds of quantum dot lasers comparing with other types of lasers. Finally, we describe the rate equation model for quantum dot lasers, simulate the model in MATLAB software package and discuss the results obtained from the simulation.

Chapter 1

Introduction

1.1 Introduction and Background

Quantum Dot Lasers have become one of the most attractive research areas in present times. They overcome many of the shortcomings of traditional quantum well lasers, and even outperform them in terms of laser characteristics. Their development has been possible due to the synthesis of semiconductor quantum dots. This chapter presents a review of the concept of QDs and their fabrication.

Quantum dots (QD) are semiconductor nanostructures (about 2~10 nm). Quantum dots are also sometimes referred to as artificial atoms as exhibit properties that are intermediate between those of bulk semiconductors and those of discrete molecules. Some of their unique properties why they are now a hot topic are:

- **Tunability** :They can be modified depending on the application as properties change with the change of their size and shape. For example, larger QDs (radius of 5–6 nm, for example) emit longer wavelengths resulting in emission colors such as orange or red. Smaller QDs (radius of 2–3 nm, for example) emit shorter wavelengths resulting in colors like blue and green, although the specific colors and sizes vary depending on the exact composition of the QD.

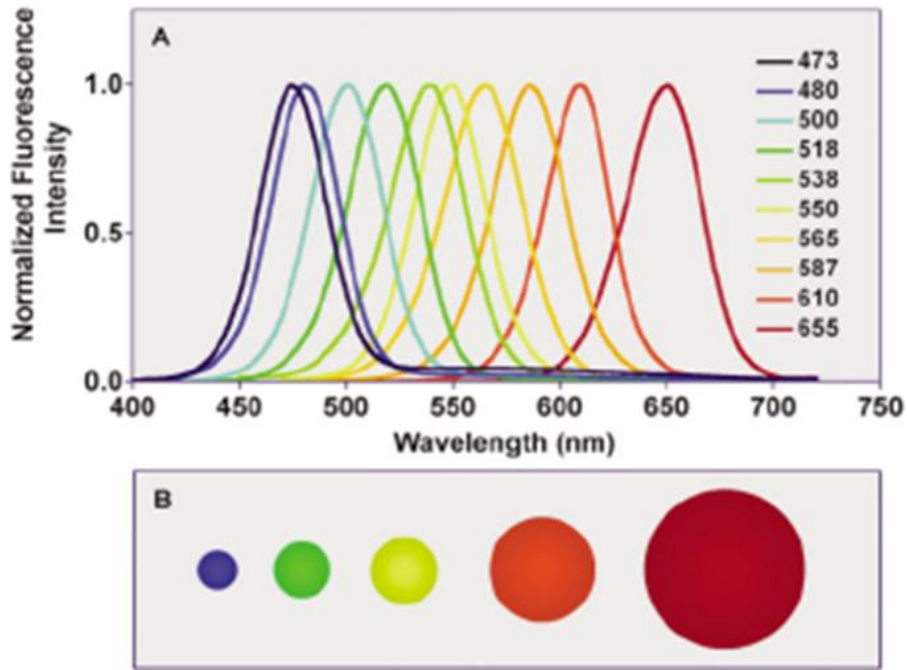


Figure 1.1:Quantum Dot wavelength and size

- **Confinement of motion** : It can be created in QDs by-
 - ✓ Electrostatic potential(e.g. doping, strain, impurities, external electrodes)
 - ✓ The presence of an interface between different semiconductor materials(e.g. in the case of self-assembled QDs)
 - ✓ The presence of semiconductor surface or by combination of these(e.g. in the case of a semiconductor nanocrystal)

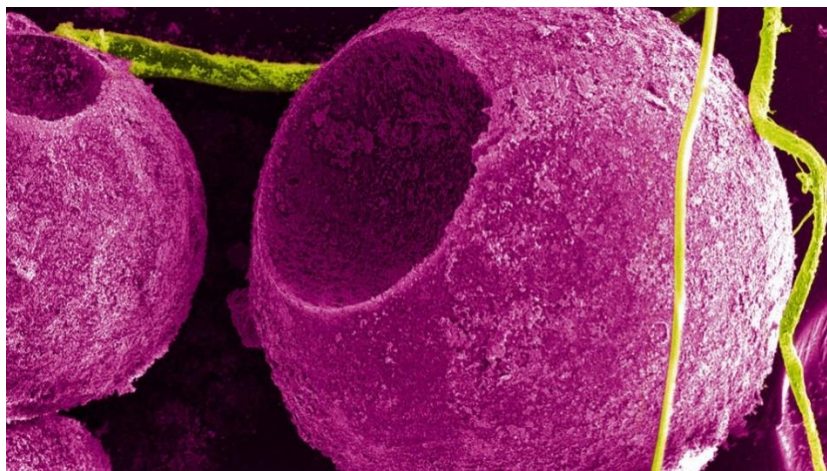


Figure 1.2: Semiconductor Quantum dot

1.2 Quantum Confinement Effects

To understand the QD concept, first of all, we should consider the quantum confinement effects on electrons. Quantum confinement occurs when one or more of the dimensions of a nanocrystal approach the Exciton Bohr radius. The concepts of energy levels, bandgap, conduction band and valence band still apply. However, the electron energy levels can no longer be treated as continuous - they must be treated as discrete.

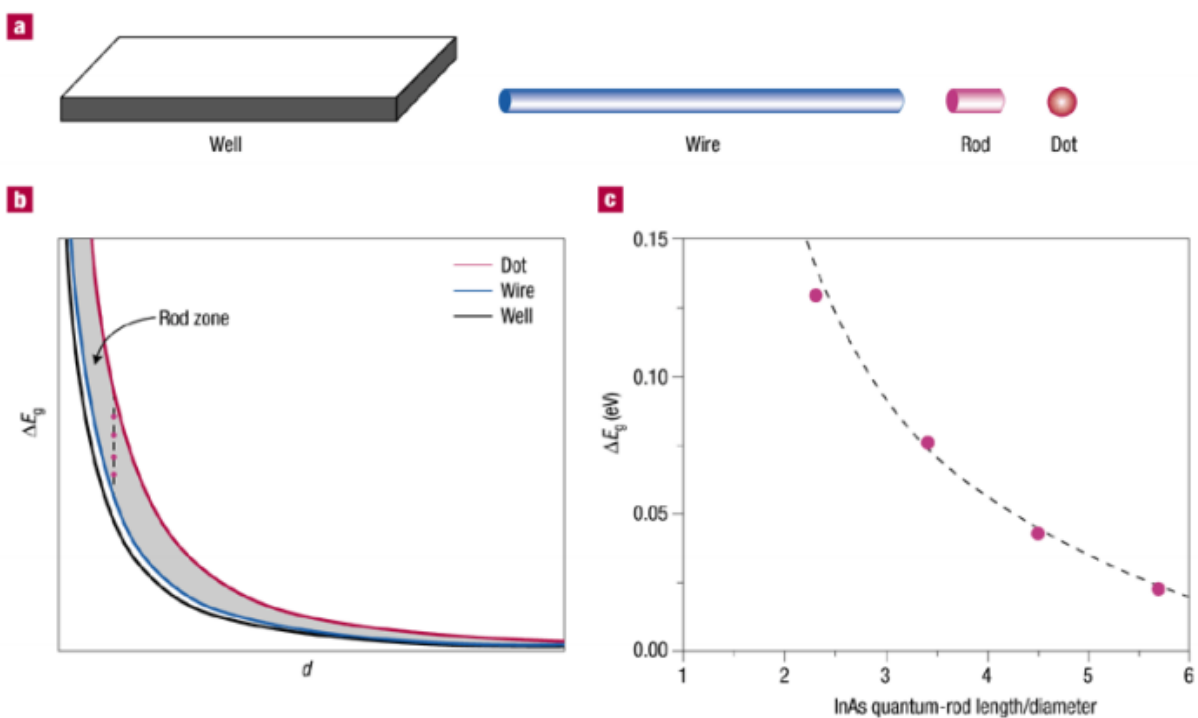


Figure 1.3: – Comparisons of quantum wells, wires, rods and dots.

a. Geometries of the different structures. **b.** Plots of E_g (the increase in the bandgap

over the bulk value) against d (the thickness or diameter) for rectangular quantum wells, cylindrical quantum wires and spherical QDs obtained from particle-in-a-box approximations. The grey area between the dot and wire curves is the intermediate zone corresponding to quantum rods. The vertical dotted line and points qualitatively represent the expected variation in the bandgap for InAs quantum rods of varying length/diameter ratio, as studied by Kan et al. 1. c. A plot of E_g against length/diameter ratio for the InAs quantum rods synthesized by Kan et al., showing the dependence of the bandgap on the shape of the quantum rods. The dotted line represents the variation expected from a particle-in-a-box approximation.

Quantum well, or quantum wire confinements give the electron at least one degree of freedom. Although this kind of confinement leads to quantization of the electron spectrum which changes the density of states, and results in one or two-dimensional energy subbands, it still gives the electron at least one direction to propagate. On the other hand, today's technology allows us to create QD structures, in which all existing degrees of freedom of electron propagation are quantized. We can think this confinement as a box of volume $d_1 d_2 d_3$. The energy is therefore quantized to: $E = E_{q1} + E_{q2} + E_{q3}$ where $E_{qn} = \frac{h^2 (q_n \pi / d_n)^2}{2m^*}$ q_1, q_2 and q_3 are the quantum numbers associated with an energy subband [6]. Since the allowed energy levels are discrete and separated, we can represent the density of states as delta functions. (Figure 3) The energy levels of a QD can be adjusted with a proper design according to the needs of the application. For instance, the addition or subtraction of just a few atoms to the QD has the effect of altering the boundaries of the bandgap. Changing the geometry of the surface of the QD also changes the bandgap energy, owing again to the small size of the dot, and the effects of quantum confinement.

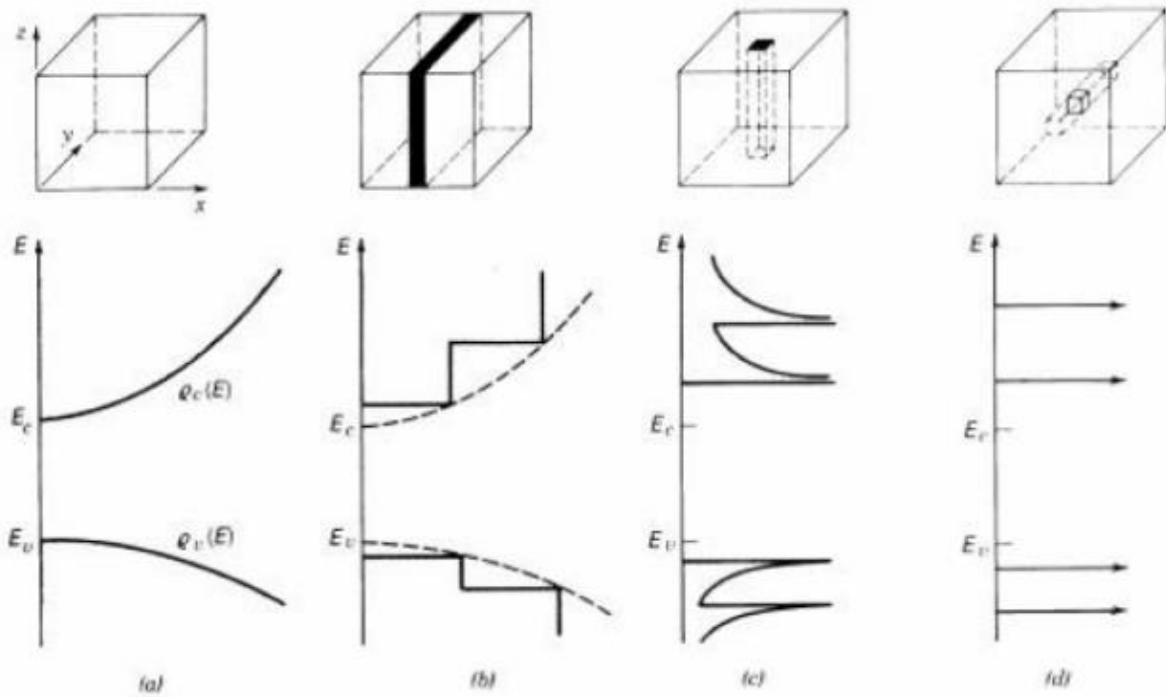


Figure 1.4: Comparison of the quantization of density of states: (a) bulk, (b) quantum well, (c) quantumwire, (d) quantum dot. The conduction and valence bands split into overlapping subbands that getsuccessively narrower as the electron motion is restricted in more dimensions.

1.3 Production Methods of Quantum Dots

- Colloidal Synthesis
- Plasma Synthesis
- Fabrication
- Viral Assembly
- Electrochemical Assembly
- Bulk Manufacture
- Heavy Metal Free Quantum Dots

1.3.1 Colloidal Synthesis

Colloidal semiconductor nanocrystals are synthesized from solutions, much like traditional chemical processes. The main difference is the product neither precipitates as a bulk solid nor remains dissolved. Heating the solution at high temperature, the precursors decompose forming monomers which then nucleate and generate nanocrystals.

There are colloidal methods to produce many different semiconductors. Typical dots are made of binary compounds such as lead sulfide, lead selenide, cadmium selenide, cadmium sulfide, cadmium telluride, indium arsenide, and indium phosphide. Dots may also be made from ternary compounds such as cadmium selenide sulfide. These quantum dots can contain as few as 100 to 100,000 atoms within the quantum dot volume, with a diameter of ~ 10 to 50 atoms. This corresponds to about 2 to 10 nanometers, and at 10 nm in diameter, nearly 3 million quantum dots could be lined up end to end and fit within the width of a human thumb. Large batches of quantum dots may be synthesized via colloidal synthesis. Due to this scalability and the convenience of bench top conditions, colloidal synthetic methods are promising for commercial applications. It is acknowledged to be the least toxic of all the different forms of synthesis.

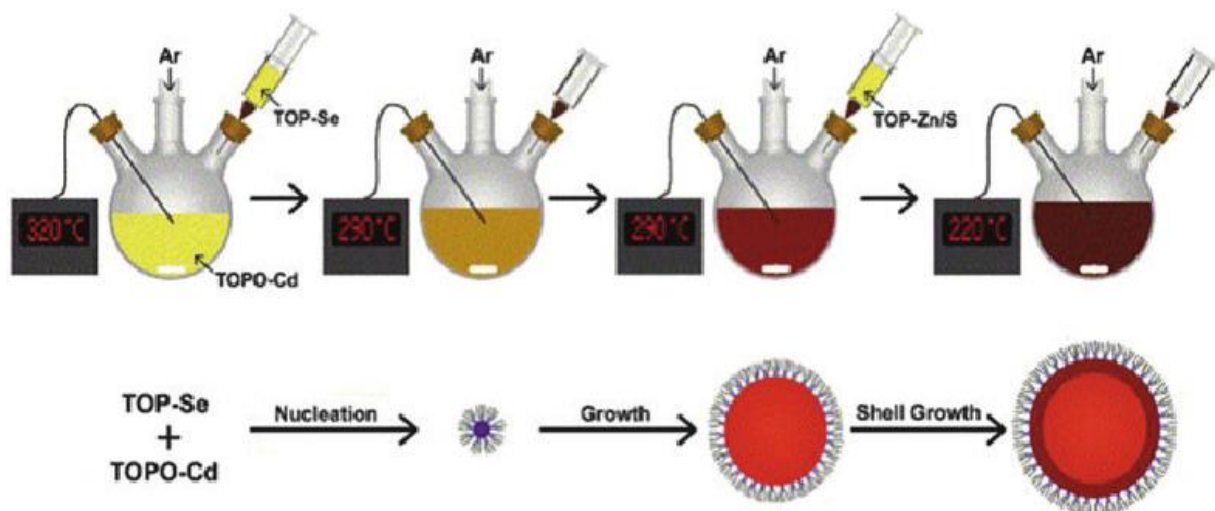


Figure 1.5: Colloidal synthesis

1.3.2 Plasma Synthesis

Plasma synthesis has evolved to be one of the most popular gas-phase approaches for the production of quantum dots, especially those with covalent bonds. For example,

silicon (Si) and germanium (Ge) quantum dots have been synthesized by using nonthermal plasma. Doping that seems quite challenging for quantum dots has also been realized in plasma synthesis. Quantum dots synthesized by plasma are usually in the form of powder, for which surface modification may be carried out.

1.3.3 Fabrication

Self-assembled quantum dots nucleate spontaneously under certain conditions during molecular beam epitaxy (MBE) and metal organic vapor phase epitaxy (MOVPE), when a material is grown on a substrate to which it is not lattice matched. The resulting strain produces coherently strained islands on top of a two-dimensional wetting layer. This growth mode is known as Stranski–Krastanov growth. The islands can be subsequently buried to form the quantum dot. This fabrication method has potential for applications in quantum cryptography (i.e. single photon sources) and quantum computation. The main limitations of this method are the cost of fabrication and the lack of control over positioning of individual dots. Individual quantum dots can be created from two-dimensional electron or hole gases present in remotely doped quantum wells or semiconductor heterostructures called lateral quantum dots. The sample surface is coated with a thin layer of resist. A lateral pattern is then defined in the resist by electron beam lithography. This pattern can then be transferred to the electron or hole gas by etching, or by depositing metal electrodes (lift-off process) that allow the application of external voltages between the electron gas and the electrodes. Such quantum dots are mainly of interest for experiments and applications involving electron or hole transport, i.e., an electrical current.

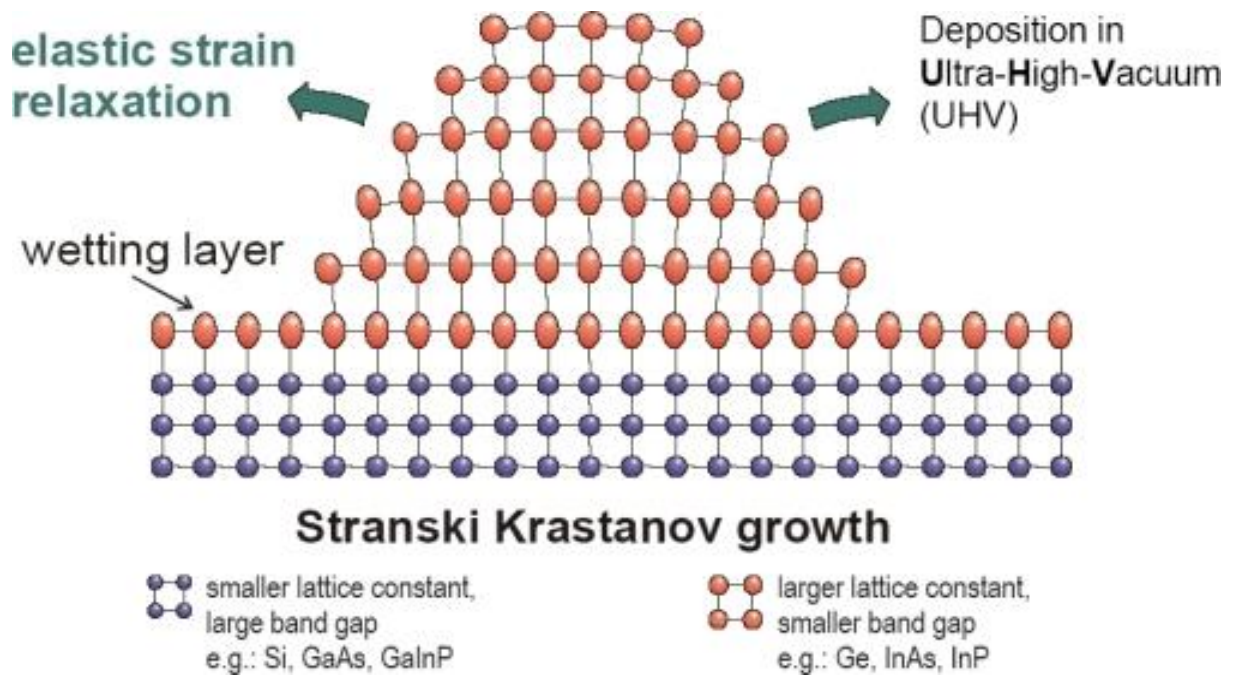


Figure 1.6:Stranski-Krastanov growth

1.3.4 Viral Assembly

Genetically engineered M13 bacteriophage viruses allow preparation of quantum dot biocomposite structures. It had previously been shown that genetically engineered viruses can recognize specific semiconductor surfaces through the method of selection by combinatorial phage display. Additionally, it is known that liquid crystalline structures of wild-type viruses (Fd, M13, and TMV) are adjustable by controlling the solution concentrations, solution ionic strength, and the external magnetic field applied to the solutions. Consequently, the specific recognition properties of the virus can be used to organize inorganic nanocrystals, forming ordered arrays over the length scale defined by liquid crystal formation. Using this information, Lee et al. (2000) were able to create self-assembled, highly oriented, self-supporting films from a phage and ZnS precursor solution. This system allowed them to vary both the length of bacteriophage and the type of inorganic material through genetic modification and selection.

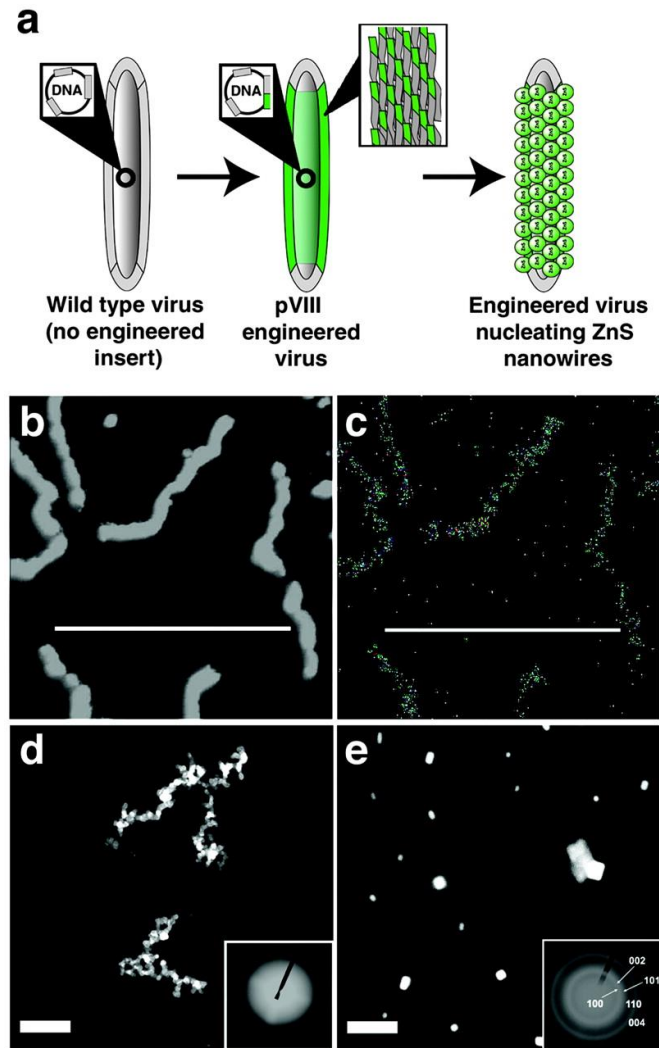


Figure 1.7: Viral assembly

1.3.5 Electrochemical Assembly

Highly ordered arrays of quantum dots may also be self assembled by electrochemical techniques. A template is created by causing an ionic reaction at an electrolyte-metal interface which results in the spontaneous assembly of nanostructures, including quantum dots, onto the metal which is then used as a mask for mesa-etching these nanostructures on a chosen substrate.

1.3.6 Bulk Manufacture

Quantum dot manufacturing relies on a process called "high temperature dual injection" which has been scaled by multiple companies for commercial applications that require large quantities (hundreds of kilograms to tones) of quantum dots. This

reproducible production method can be applied to a wide range of quantum dot sizes and compositions.

The bonding in certain cadmium-free quantum dots, such as III-V-based quantum dots, is more covalent than that in II-VI materials, therefore it is more difficult to separate nanoparticle nucleation and growth via a high temperature dual injection synthesis. An alternative method of quantum dot synthesis, the “molecular seeding” process, provides a reproducible route to the production of high quality quantum dots in large volumes. The process utilizes identical molecules of a molecular cluster compound as the nucleation sites for nanoparticle growth, thus avoiding the need for a high temperature injection step. Particle growth is maintained by the periodic addition of precursors at moderate temperatures until the desired particle size is reached. The molecular seeding process is not limited to the production of cadmium-free quantum dots; for example, the process can be used to synthesize kilogram batches of high quality II-VI quantum dots in just a few hours.

Another approach for the mass production of colloidal quantum dots can be seen in the transfer of the well-known hot-injection methodology for the synthesis to a technical continuous flow system. The batch-to-batch variations arising from the needs during the mentioned methodology can be overcome by utilizing technical components for mixing and growth as well as transport and temperature adjustments. For the production of CdSe based semiconductor nanoparticles this method has been investigated and tuned to production amounts of kg per month. Since the use of technical components allows for easy interchange in regards of maximum through-put and size, it can be further enhanced to tens or even hundreds of kilograms.

In 2011 a consortium of U.S. and Dutch companies reported a "milestone" in high volume quantum dot manufacturing by applying the traditional high temperature dual injection method to a flow system.

On January 23, 2013 Dow entered into an exclusive licensing agreement with UK-based Nanoco for the use of their low-temperature molecular seeding method for bulk manufacture of cadmium-free quantum dots for electronic displays, and on September 24, 2014 Dow commenced work on the production facility in South Korea capable of producing sufficient quantum dots for "millions of cadmium-free televisions and other devices, such as tablets". Mass production is due to commence in mid-2015. On 24 March 2015 Dow announced a partnership deal with LG Electronics to develop the use of cadmium free quantum dots in displays.

1.3.7 Heavy metal-free quantum dots

In many regions of the world there is now a restriction or ban on the use of heavy metals in many household goods, which means that most cadmium based quantum dots are unusable for consumer-goods applications.

For commercial viability, a range of restricted, heavy metal-free quantum dots has been developed showing bright emissions in the visible and near infra-red region of the spectrum and have similar optical properties to those of CdSe quantum dots. Among these systems are InP/ZnS and CuInS/ZnS, for example.

Peptides are being researched as potential quantum dot material. Since peptides occur naturally in all organisms, such dots would likely be nontoxic and easily biodegraded.

1.4 Development of Quantum Dot Lasers

The laser operation is based on producing radiative emission by coupling electrons and holes at nonequilibrium conditions to an optical field. The advantages of quantum well lasers on traditional lasers first predicted in 1970s (*Dingle and Henry 1976*), and first quantum well lasers which were very inefficient were demonstrated at those dates (*van der Ziel et al. 1975*). The advantages recognized were:

- The confinement and nature of the electronic density of states result in more efficient devices operating at lower threshold currents than lasers with bulk active layers. The laser threshold current density can be reduced by decreasing the thickness of the active layer.
- Discrete energy levels provide a means of "tuning" the resulting wavelength of the material. Since the thickness of the quantum well depends on the desired spacing between energy levels, tuning can be done by changing the quantum well dimensions or thickness. For energy levels of greater than a few tens of meV's, the critical dimension is

approximately a few hundred angstroms.

The inefficiency of quantum well lasers were eliminated in 1980s by the use of new materials growth capabilities (molecular beam epitaxy), and optimization of the heterostructure laser design.

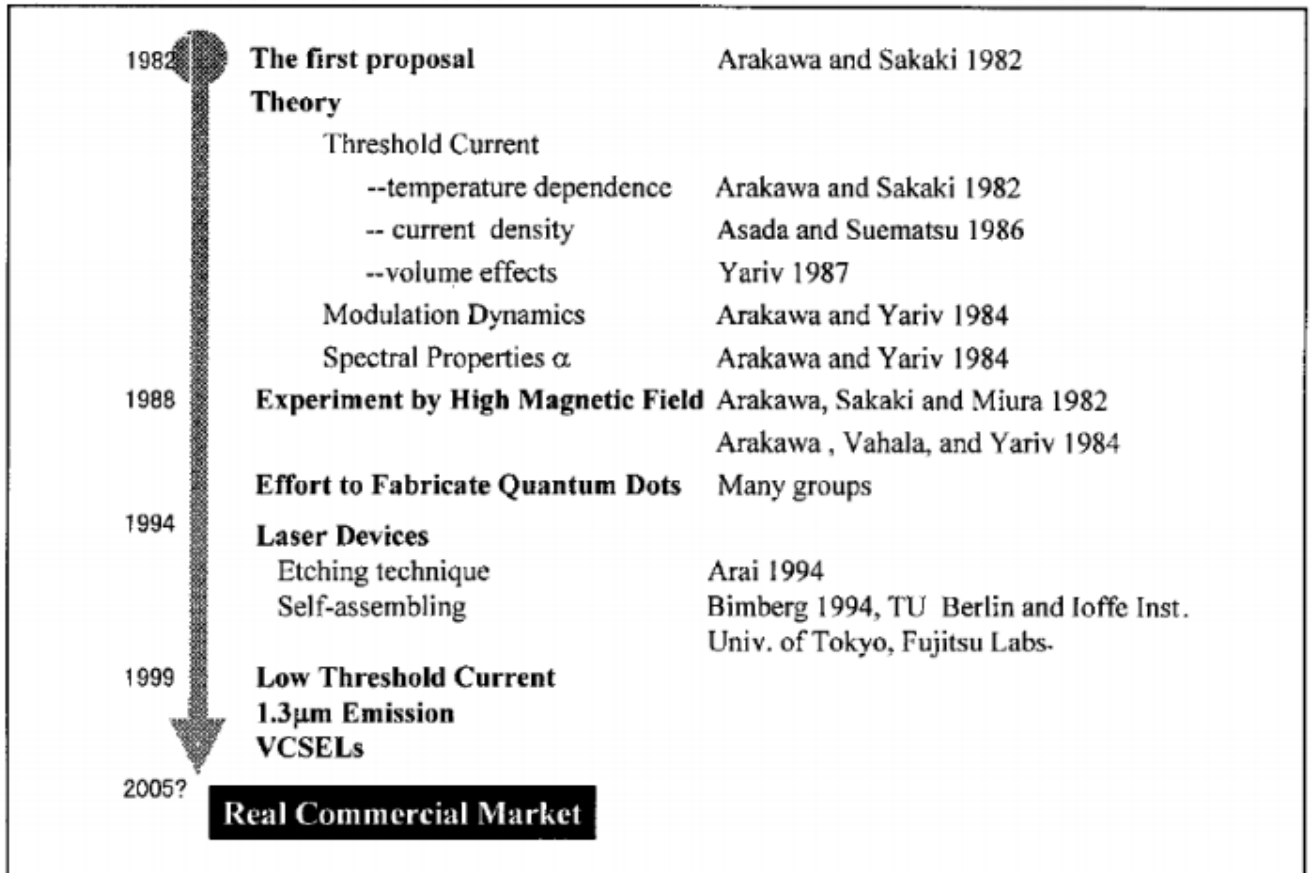


Figure 1.8:The historical evolution of QD lasers from the beginning.

Since the quantum confinement in a QD is in all three dimensions, tunability of a quantum dot laser (QDL) is higher than a quantum well laser (QWL). The concept of semiconductor QDs was proposed for semiconductor laser applications by Arakawa and Sakaki in 1982, predicting suppression of temperature dependence of the threshold current. Henceforth, reduction in threshold current density, reduction in total threshold current, enhanced differential gain and high spectral purity/no-chirping were theoretically discussed in 1980's.

Chapter 2

Quantum Dot Application in LASER

2.1 Introduction

Semiconductor lasers are the main components in a host of widely used useful technological products like compact disk players and laser printers, and they will play critical roles in optical communication schemes. The basis of laser operation depends on the creation of nonequilibrium populations of electrons and holes, and coupling of electrons and holes to an optical field, which will stimulate radiative emission. Greater benefits have been predicted for lasers with quantum dot active layers. Arakawa and Sakaki (1982) predicted in the early 1980s that quantum dot lasers should exhibit performance that is less temperature-dependent than existing semiconductor lasers, and that will in particular not degrade at elevated temperatures. Other benefits of quantum dot active layers include further reduction in threshold currents and an increase in differential gain-that is, more efficient laser operation (Asada et al. 1986).

2.2 LASER

The letters in the word laser stand for Light Amplification by Stimulated Emission of Radiation. A laser is an unusual light source. Lasers produce a very narrow beam of light. This type of light is useful for lots of technologies and instruments.

2.2.1 Components of a LASER

Every LASER consists of three basic components. These are -

1. Lasing material or active medium.
2. External energy source.
3. Optical resonator.

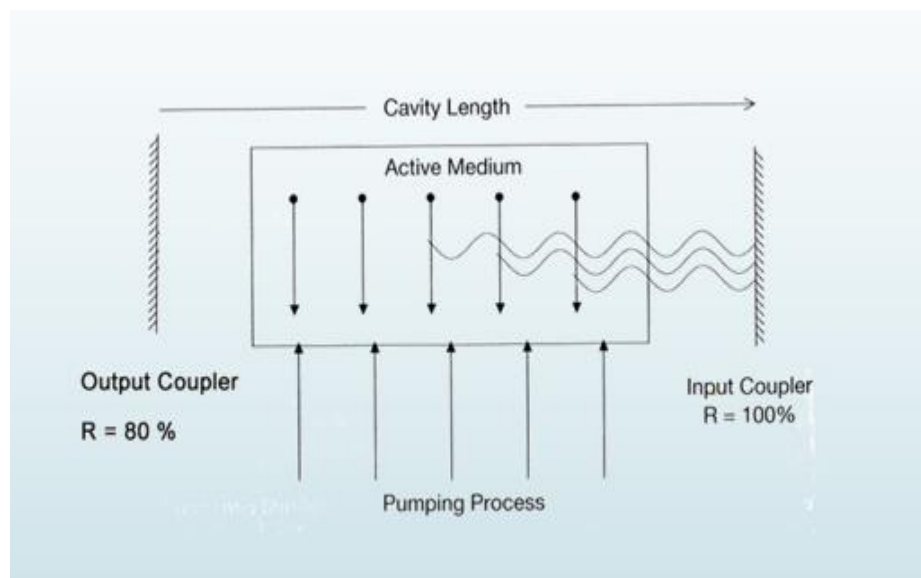


Figure 2.1: Lasing Operation.

2.2.2 Lasing material or active medium

The active medium is excited by the external energy source (pump source) to produce the population inversion. In the gain medium that spontaneous and stimulated emission of photons takes place, leading to the phenomenon of optical gain, or amplification. Semiconductors, organic dyes, gases (He, Ne, CO₂, etc), solid materials (YAG, sapphire (ruby) etc.) are usually used as lasing materials and often LASERs are named for the ingredients used as a medium.

2.2.3 External energy source

The excitation source, pump source provides energy which is needed for the population inversion and stimulated emission to the system. Pumping can be done in two ways - electrical discharge method and optical method. Examples of pump sources are electrical discharges, flash lamps, arc lamps, light from another laser, chemical reactions etc.

2.2.4 Optical resonator

Resonator guide basically provides the guidance about the simulated emission process. It is induced by high-speed photons. Finally, a laser beam will be generated. In most of the systems, it consists of two mirrors. One mirror is fully reflective and other is partially reflective. Both the mirrors are set up on optic axis, parallel to each other. The active medium is used in the optical cavity between the both mirrors. This arrangement only filters those photons which came along the axis

and others are reflected by the mirrors back into the medium, where it may be amplified by stimulated emission.

2.3 Why Quantum Dot in LASER

1. The quantum dot active region can be engineered to operate at different wavelengths by varying dot size and composition.
2. This allows them to be operated at wavelengths not possible using semiconductor laser technology.
3. Quantum dot lasers have lower threshold current making them more efficient as compared to quantum well laser.
4. Better performance at elevated temperature as less dependent on temperature variations.

2.4 Q. Dot Laser vs. Q. Well Laser

In order for QD lasers compete with QW lasers:

- A large array of QDs since their active volume is small
- An array with a narrow size distribution has to be produced to reduce inhomogeneous broadening
- Array has to be without defects
 - ✓ May degrade the optical emission by providing alternate nonradiative defect channels
- The phonon bottleneck created by confinement limits the number of states that are efficiently coupled by phonons due to energy conservation

- ✓ Limits the relaxation of excited carriers into lasing states
- ✓ Causes degradation of stimulated emission
- ✓ Other mechanisms can be used to suppress that bottleneck effect (e.g. Auger interactions)

2.5 Bottlenecks

Apart from all the advantages of using Quantum Dot there are also some disadvantages. Such as:

1. Lack of uniformity of QD distribution.
2. Quantum Dots density is insufficient.
3. The lack of good coupling between QD and Substrate.

2.6 Development of Quantum Dot Lasers

The laser operation is based on producing radiative emission by coupling electrons and holes at nonequilibrium conditions to an optical field. The advantages of quantum well lasers on traditional lasers first predicted in a few years back, first quantum dot lasers were very inefficient. The advantages recognized were:

- The confinement and nature of the electronic density of states result in more efficient devices operating at lower threshold currents than lasers with bulk active layers. The laser threshold current density can be reduced by decreasing the thickness of the active layer.
- Discrete energy levels provide a means of "tuning" the resulting wavelength of the

material. Since the thickness of the quantum well depends on the desired spacing between energy levels, tuning can be done by changing the quantum well dimensions or thickness. For energy levels of greater than a few tens of meV's, the critical dimension is approximately a few hundred angstroms.

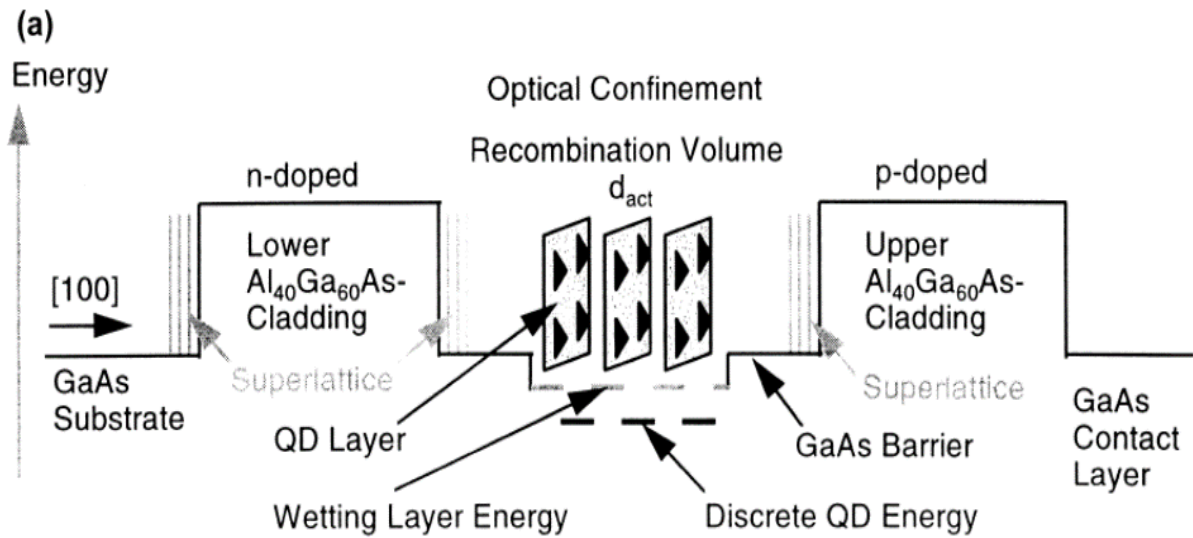


Figure 2.2: LASER Using QD Layer.

2.7 Predicted Advantages of Quantum Dot LASERS

1. Emits light at wavelengths determined by the energy levels of the dots, rather than the band gap energy. Thus, they offer the possibility of improved device performance and increased flexibility to adjust the wavelength.
2. Has the maximum material gain and differential gain, at least 2-3 orders higher than QW lasers
3. Advantages of small volume:
 - a. Low power high frequency operation,

- b. Large modulation bandwidth,
 - c. Small dynamic chirp,
 - d. Small linewidth enhancement factor,
 - e. Low threshold current.
4. Shows superior temperature stability of the threshold current. The threshold current is given by the relation:
- $$I_{\text{threshold}}(T) = I_{\text{threshold}}(T_{\text{ref}}) \cdot \exp\left(\frac{T - (T_{\text{ref}})}{T_0}\right)$$
- where T is the active region temperature, (T_{ref}) is the reference temperature, and (T_0) is an empirically-determined "characteristic temperature", which is itself a function of temperature and device length. In QDLs T_0 can be high, because one can effectively decouple electron-phonon interaction by increasing the inter-subband separation. This leads to undiminished room-temperature performance without external thermal stabilization.
5. QD lasers suppress the diffusion of non-equilibrium carriers, resulting in reduced leakage from the active region

2.8 Different Types of Quantum Dot Lasers

2.8.1 High speed quantum dot lasers

There are several epitaxials were proposed to get the predicted advantages of QD lasers, among them are: overgrowth of QDs with quantum well layers, stacking of quantum dots, close stacking of quantum dots leading to the vertical coupling of quantum dot layers, p-doping of the GaAs barrier layers.

2.8.2 Directly modulated QDL:

Being the key point of the fiber-based datacom application, directly modulated quantum dot lasers could convert electrical signals into digital optical signals at the rate of around 10Gb/s. The modulation speed needs to be further improved, the power consumption should be reduced and the temperature performance needs to be better.

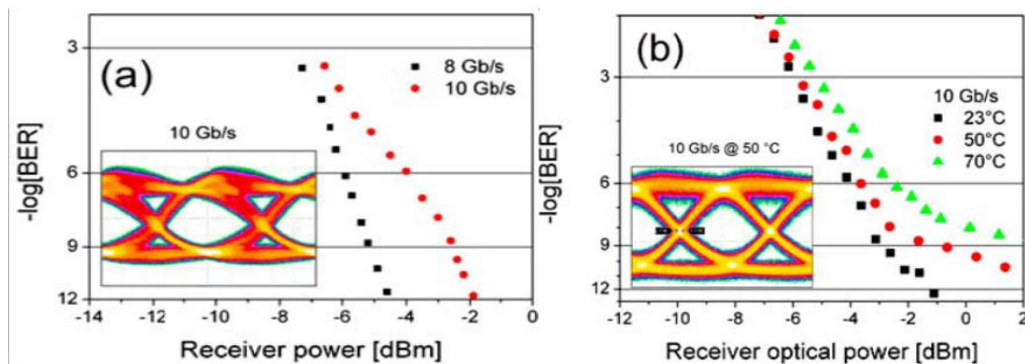


Figure 2.3: BER measurement of QD laser module at 8 Gb/s and 10 Gb/s (a) and at 10 Gb/s for different temperatures (b), inset shows the corresponding eye patterns.

2.8.3 Mode-Locked QDL

With the applications of Mode-Locked quantum dot lasers, several advantages could be received: short optical pulses, narrow spectral width with a small footprint device. Besides, Mode-Locked quantum dot lasers are able to provide a much broader gain spectrum ($>50\text{nm}$), longer cavities (approximately 1cm), sub-ps width and a very low

α factor which leads to low chirp.

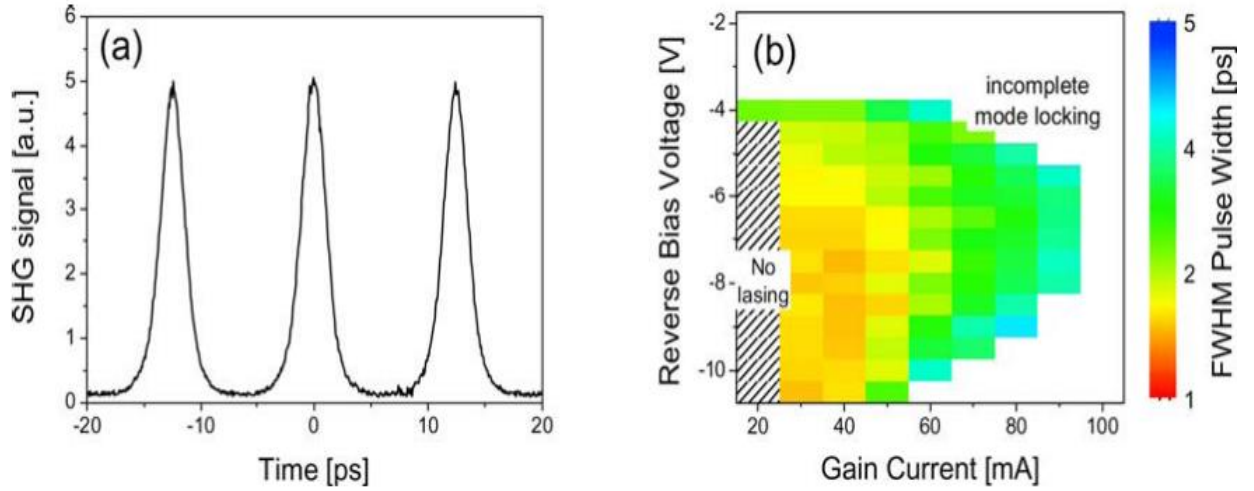


Figure 2.4: Autocorrelation trace of a passively mode-locked quantum dot laser at 1.3 μm and 80 GHz repetition rate. The side peaks correspond to the cross-correlation of two successive pulses, while the middle peak presents the autocorrelation of a pulse (a). Field scan of auto-correlation traces with color coded FWHM pulse widths of a 80 GHz passively mode-locked QD laser. Three regimes of operation can be distinguished (b).

2.8.4 InP based QDL

Compared with QW lasers, the emission wavelength of the InP based quantum dot lasers is much lower (0.2nm/K compared to 0.55nm/K). This property could allow this kind of quantum dot lasers operate within a much wider temperature range.

Although there still exist some limitations in speed due to the inhomogeneous linewidth broadening, the data transmission could still be possibly over 10Gb/s for InP based quantum dot lasers.

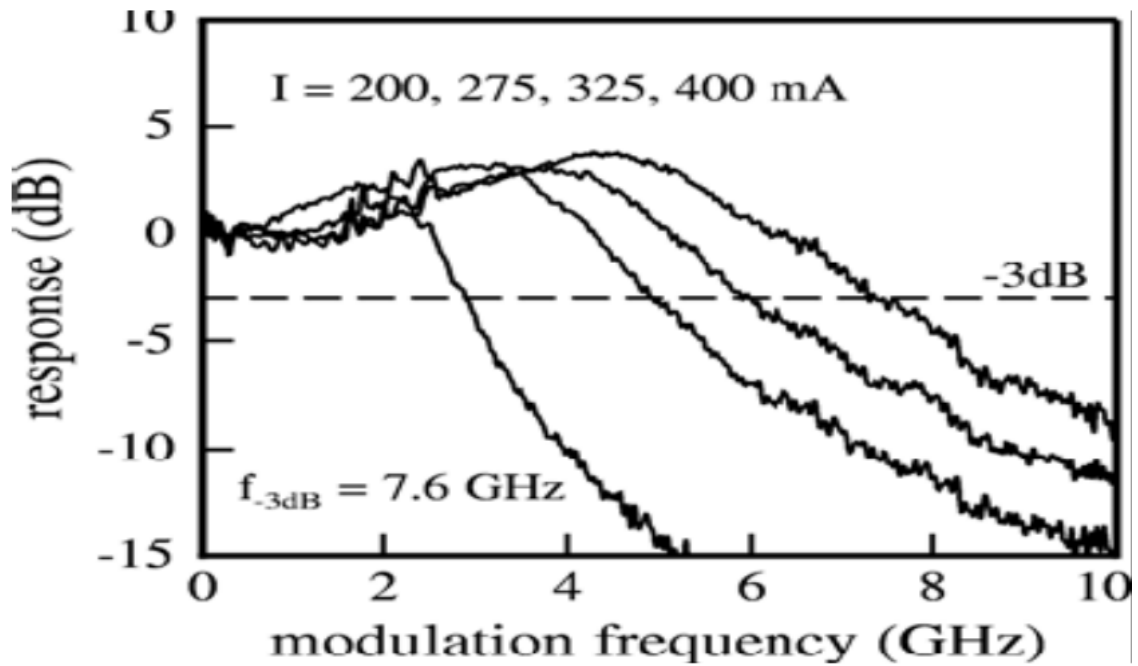


Figure 2.5: Small signal modulation response for a QDash DFB laser at four different pulsed ($10 \mu\text{s}$ pulses at a duty cycle of 2%) bias levels.

2.8.5 High power QDL

With several promising properties of the quantum dot materials, it is widely realized that quantum dot lasers are able to get a good power performance. The advantages of quantum dot materials to be suitable applied to high power application fields are: zero linewidth enhancement factor, the free geometric parameters of the quantum dots, e. g. quantum dots size, dots density and size distribution could allow to get the gain without considering the material composition. Extra expensive cooling by Peltier elements is then not needed.

2.8.6 QDLs for coolerless pump sources.

The devices with these properties are recently developed based on the GaInAs/Ga(Al)As QD layers emitting at 920nm. In this research, the size of the quantum dot is reduced by modifying the growth parameter and In composition with a constant emission wavelength of the transition. A power splitting of 65eV could be received at room temperature wavelength of 920nm with the size reduced quantum dot structures.

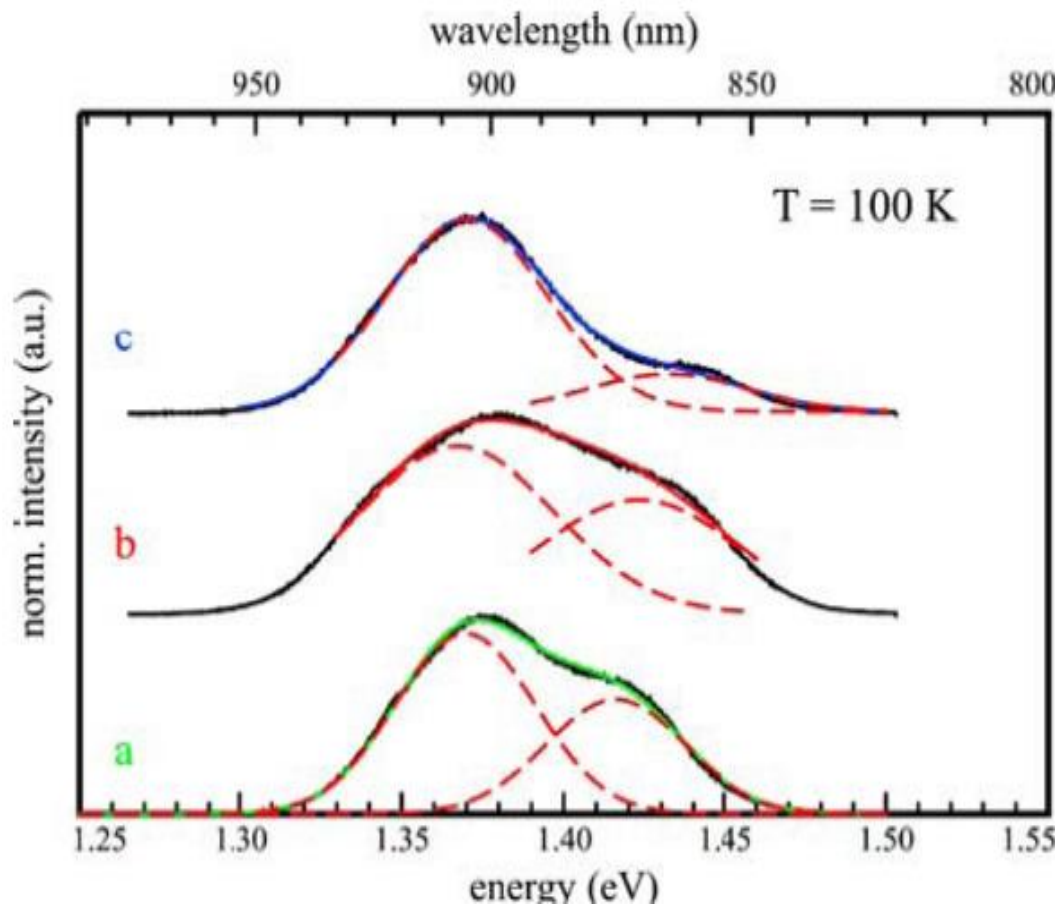


Figure 2.6: PL spectra of dot layers with different dot sizes resulting in different transition energy splittings between fundamental and first excited state transitions (a=47meV, b= 56 meV, c = 65 meV).

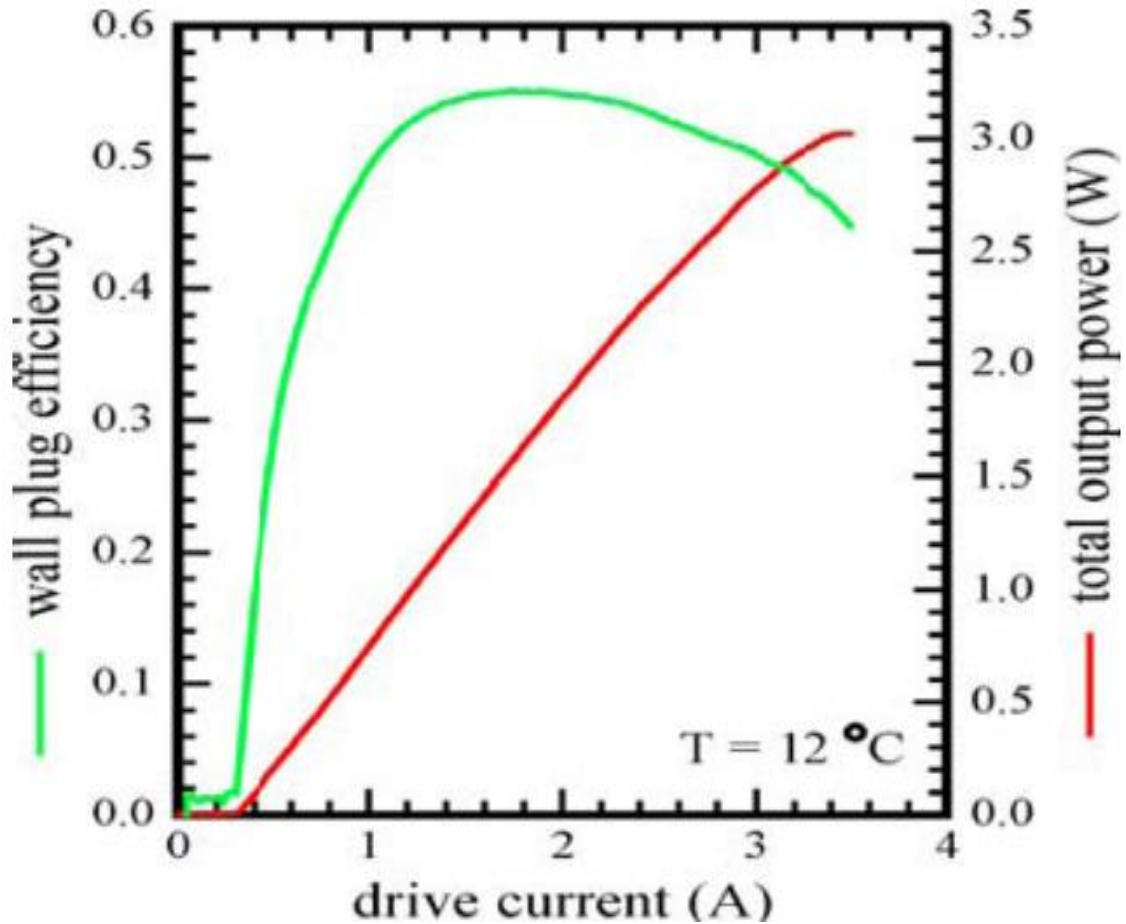


Figure 2.7: Total output power and wall-plug efficiency of a quantum dot high power laser with 1 mm cavity length and 100 μm broad contact stripes. The facets are cleaved without coatings. Maximum cw output power of 3.02 W and a maximum wall-plug efficiency of 55% at 1.5 W are obtained.

2.8.7 Single mode tapered lasers

New device geometry is used to get a similar performance as multi-mode emitting devices. Such kind of lasers enables the amplification of the single mode during the propagation. Compared with quantum well lasers, the wavelength shift is smaller due to the better temperature performance (temperature sensitivity).

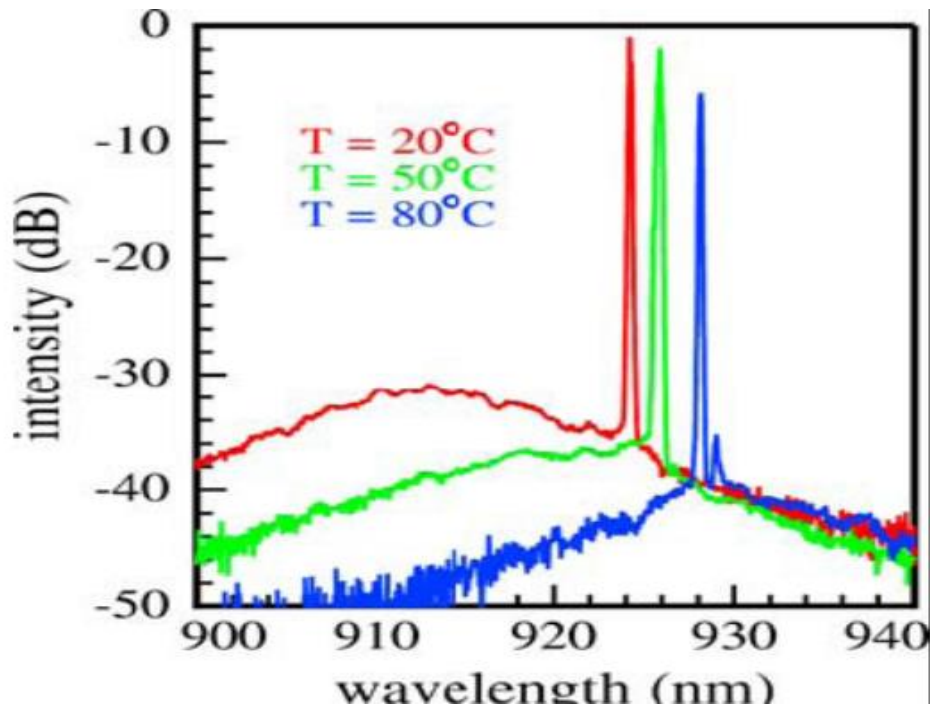


Figure 2.8: Emission spectra for 3 different temperatures of a single mode emitting QD tapered laser are shown.

2.9 Applications of Quantum Dot LASER

1. QD lasers are used in Monolithically integrated widely tunable narrow-linewidth light source for the C+ band based.
2. Also it is used for fabricating Integrated Silicon Nitride Micro-disk Lasers.
3. It has application for Laser-patterned Array with Aerosol-jet Printing for Novel White Light Source.
4. It is used in Compact All-Quantum-Dot-Based Tunable THz Laser Source.
5. Recently it is used for Optical data communications, Optical networks Optical LANs.

Chapter 3

Modeling of Quantum Dot Lasers

3.1 The Ridge Waveguide QD Laser

In this section, a theoretical model will be created for a system containing a ridge waveguide QD laser which enables simulations of the turn-on dynamics. The approach is to use a setup of rate equations (REs) to compute the carrier population densities and the photon population densities in the system at a series of time steps. The structure of the laser is seen in figure 3.1A. For pumping the laser a current is set to flow down through the top of the ridge. The associated area current density, $j(t)$, is a function of time. The current will supply the ridge material with electrons in the conduction band and holes in the valence band. In the ridge material, a_L numbers of QD layers are embedded on top of each other parallel to the ridge top face. The ridge laser has a ground area of $A = 4\mu\text{m} \cdot 1\text{ mm}$, and hence this is the normalisation area of the WL. Each QD layer has a QD density of $N^{QD}/2$, and each QD covers an area of γ_{xy} . At the two end facets of the ridge, a mirror is placed with the reflective coefficients r_1 and r_2 , respectively. It is assumed that non-radiative scattering processes within the WL and the QD elapse much faster than the radiative processes, and consequently a two-level system with the groundstate in the QD and a state in the WL is used as an approximation to the real many-state system. This leads to a system with only the non-radiative transition between the state in the WL and the groundstate QD in the valence band and the conduction band, respectively and the two processes of recombination, see figure 3.1B.

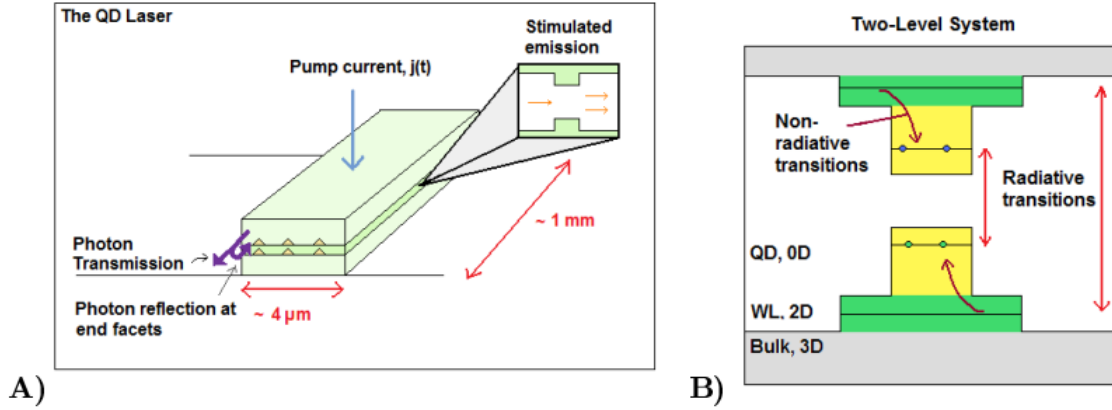


Figure 3.1: A) The ridge waveguide QD laser. The current flows down through the top of the ridge. The QDs are illustrated as triangles. At the mirrors, a part of the photons will be transmitted and a part will be reflected. The photons inside the ridge travelling in the longitudinal direction will be reflected and accumulate. This accumulation leads to an increase in the stimulated emissions in the QDs. B) The four energy states of the two-level system. The two relaxation processes, and the two recombination processes are illustrated.

3.1.1 The Rate Equation Model

The two-level system has four carrier populations: The population densities of electrons in the QD and WL termed n_e and w_e , respectively, and the population densities of holes in the QD and WL termed n_h and w_h , respectively. A fifth population density of the emitted photons in the longitudinal direction is needed, termed n_{ph} . All densities are with respect to the WL normalisation area. The rate equation system (RES) consists of five coupled first order differential equations, one equation for the rate of each of the mentioned population densities:

$$\dot{n}_e = -\frac{1}{\tau_e} n_e + S_e^{in} N^{QD} - R_{ind}(n_e, n_h) - R_{sp}(n_e, n_h) \dots \dots \dots (1)$$

$$\dot{n}_h = -\frac{1}{\tau_h} n_h + S_h^{in} N^{QD} - R_{ind}(n_e, n_h) - R_{sp}(n_e, n_h) \dots \dots \dots (2)$$

$$\dot{w}_e = \frac{j(t)}{e_0} + \frac{n_e N^{WL}}{\tau_e N^{QD}} - S_e^{in} N^{WL} - \widetilde{R}_{sp}(w_e, w_h) \dots \dots \dots (3)$$

$$\dot{w}_h = \frac{j(t)}{e_0} + \frac{n_h}{\tau_h} \frac{N^{WL}}{N^{QD}} - S_h^{in} N^{WL} - \widetilde{R}_{sp}(w_e, w_h) \dots (4)$$

$$\dot{n}_{ph} = -2 \kappa n_{ph} + \Gamma R_{ind}(n_e, n_h) + \beta R_{sp}(n_e, n_h) \dots (5)$$

The first term in Eqs. (3) and (4), $\frac{j(t)}{e_0}$, where e_0 is the elementary charge, is the source term for the carriers and is related to the current injected into the WL. In general the first four equations have two types of terms: The terms containing the non-radiative scattering rates, S_e^{in} , S_h^{in} , including the scattering times τ_e and τ_h , and the terms containing the radiative scattering rates, R_{sp} , \widetilde{R}_{sp} and R_{ind} .

The scattering times are defined by:

$$\tau_e = (S_e^{in} + S_e^{out})^{-1}; \tau_h = (S_h^{in} + S_h^{out})^{-1} \dots (6)$$

where S_e^{in} and S_h^{in} are the scattering rates from the WL to the QD for electrons and holes, respectively. Likewise S_e^{out} and S_h^{out} are the scattering rates from the QD to the WL. To understand the terms $-\frac{1}{\tau_e} n_e + S_e^{in} N^{QD}$ and the coherence to the in- and out-scattering rates the general term:

$$\dot{f}_{e/h} = (1 - f_{e/h}) S_{e/h}^{in} - f_{e/h} S_{e/h}^{out} = -\frac{f_{e/h}}{\tau_{e/h}} + S_{e/h}^{in} \dots (7)$$

is studied. $f_{e/h}$ is the probability of finding the electron/hole in a QD state and in consequence $(1 - f_{e/h})$ is the probability of finding the electron/hole in the WL. For $f_{e/h} = 1$ the QD state is filled and the out-scattering is at maximum while the in-scattering is at minimum, and vice versa for $f_{e/h} = 0$. In Eq. (1) it is used that $n_e = f_e N^{QD}$ together with the $f_{e/h}$ expression, and analogous expressions are used for Eqs. (2)-(4). The non-radiative scattering rates are calculated by a summation over all WL states. These summations lead to bulky calculations that must be executed at each time step. The scattering rates take into account two types of scatterings: The pure electron-electron and hole-hole scatterings, and the mixed electron-hole scattering. For the pure processes, S_e^{in} and S_e^{out} are functions of the electron population in the WL, i.e. of w_e , and S_h^{in} and S_h^{out} are functions of the hole population in the WL, i.e. of w_h . To incorporate the mixed processes in the scattering rates a constant $g_c = w_h/w_e$ is defined

from the values of w_e and w_h when the system is in steady-state. The simulations are repeated from $t = 0$ to steady-state until the value of g_c stabilises. Another method is to update the value g_c at each time step. These two methods, the self-consistent g_c -method and the dynamic g_c -method, will be used in the following. The primary method is the self-consistent method since it best correlates with the experimental data in [8] in terms of turn-on dynamics. The second type of terms in the first four equations are the rates for the radiative processes. There are rates for the spontaneous emissions in the QD and WL, respectively:

$$R_{sp}(n_e, n_h) = \frac{W}{N^{QD}} n_e n_h, \widetilde{R}_{sp}(w_e w_h) = \frac{W}{N^{WL}} w_e w_h \dots \dots \dots (8)$$

where N^{WL} is the effective density of states in the WL. The rates are proportional to the Einstein coefficient W . The spontaneous emission rates depend on the populations of the electrons and holes that can recombine in either the QD or WL. It is the spontaneous processes that create the first photons, but when the population density n_{ph} increases, the induced emission process in the QD becomes predominant. The mirrors at the end facets accumulate photons in the ridge structure travelling in the longitudinal direction. Photons emitted in other directions leave the structure. When a photon travels back and forth between the mirrors it will induce stimulated emission. Photons emitted by this carrier-photon interaction has the same momentum as the incoming photon further building up the number of photons in the longitudinal direction. The rate of the stimulated emission is:

$$R_{ind}(n_e, n_h) = WA(n_e + n_h - N^{QD})n_{ph} \dots \dots \dots (9)$$

The partial reflection at the end facets and the radiative rate influence the photon population in the longitudinal direction, as seen in Eq. (5). The first term, $-2\kappa n_{ph}$, describes a loss, where $\kappa = (\kappa_{int} - \frac{\ln(r_1 r_2)}{2L}) \frac{c}{\sqrt{\epsilon_{bg}}}$ with L as the length of the cavity, c as the speed of light and ϵ_{bg} as the background dielectric constant. κ_{int} is related to internal loss of photons, owing to imperfections in the material and material absorption. The second term in κ is due to transmission of light through the mirrors. Since the argument of \ln is less than unity, this leads to an overall negative term in

Eq. (5), i.e., photons escaping the cavity are accounted as a loss in the photon density population. It is evident that the loss term and hereby the escaping photons from the laser are proportional to n_{ph} . By plotting n_{ph} as a function of time the turn-on dynamics of the laser can be studied. The next term in Eq. (5), $\Gamma R_{ind}(n_e, n_h)$, is the increase in the photon population density due to the induced emission. The optical confinement factor is given by $\Gamma = N^{QD} a_L \gamma_{xy} \Gamma_z$, where Γ_z is the vertical confinement factor. The optical confinement factor is the ratio of the active area of the optical mode and the electronic active area. Γ_z is a constant related to the design of the ridge expressing the interaction between the optical mode and the electrons in the active area of the structure. The last term in Eq. (5), $\beta R_{sp}(n_e, n_h)$, is related to spontaneous emission. β is the probability that the spontaneous emission will be in the longitudinal direction where it will be a part of the laser mode. At last it is worth noticing that the spontaneous emissions in the WL do not contribute to the laser mode even though some of the photons are emitted in the longitudinal direction. Only photons with wavelengths, of which L is a multiple, are confined in the cavity [8]

Chapter 4

Simulation of RES model

4.1 Simulation of rate equations in Matlab

We tried to simulate the rate equations in MATLAB. Simulation of rate equations in MATLAB gives us an elaborate and detailed study and analysis of quantum dot lasers. We can also study the turn on characteristics and behavior of quantum dot lasers until it reaches steady state.

Results of the simulation of rate equations in MATLAB is explained here.

4.2 QD layer electron density vs Time:

This simulation is shown for the electron population density in quantum dot layer vs time. The results are obtained from numerical simulations for dynamic scattering rates shown in the figure 4.1.

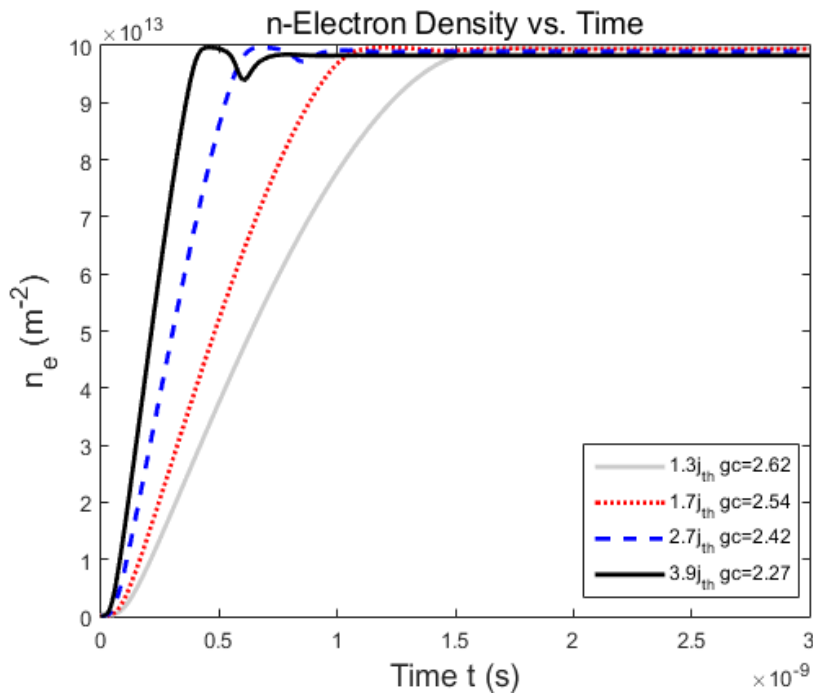


Figure 4.1: QD electron density vs time.

From the figure, curves are shown for different pump currents ranging from $1.3j_{th}$ to $3.9j_{th}$. For different pumping currents different colors are indicated. It can be seen that for higher pump currents, photon peaks appear faster which means it reaches steady state faster. If we compare the graphs of $1.3j_{th}$ and $3.9j_{th}$, we can see that it takes substantially less time to reach steady-state among these threshold currents. We found out that this happens due to the fact that for higher currents higher number of electrons are being fed to the system in a short duration of time. As it forces the system to begin emission earlier. Because of that the first peak appears faster for high pumping currents.

4.3 QD layer hole density vs Time:

In this case, simulation is shown for the hole population density in quantum dot layer vs time. Simulation of hole density in quantum dot layer is a little bit similar to electron density vs time. In this case also curves are shown for different pumping currents ranging from $1.3j_{th}$ to $3.9j_{th}$ shown in the figure 4.2.

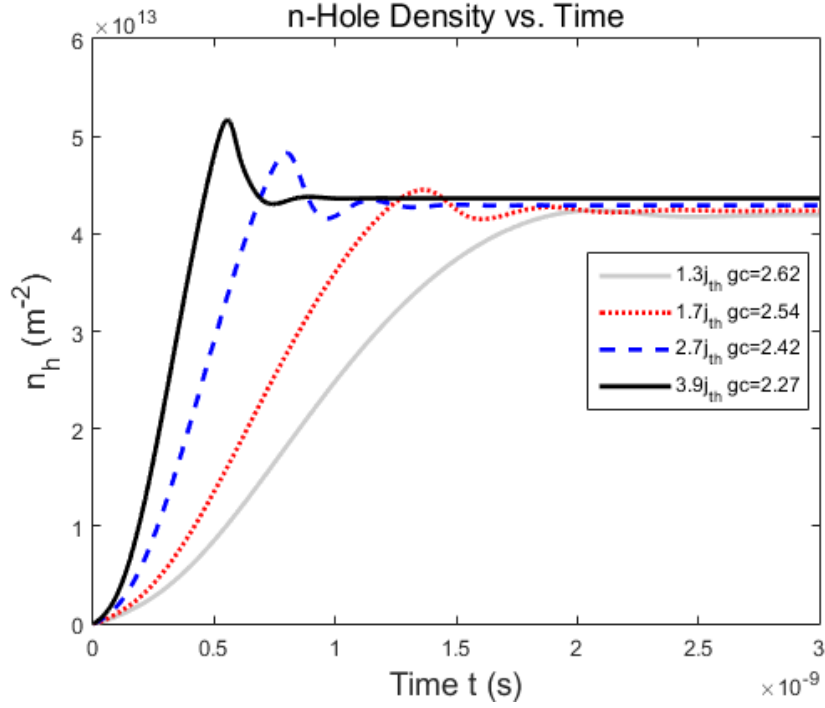


Figure 4.2: Curves simulated for hole density in QD layer vs time.

In this case also for higher pumping currents steady state reaches faster. This happens because of the fact that for high pumping currents higher number of holes are fed to the system causing the system to commence emission earlier.

4.4 Wetting layer electron density vs time:

After simulating the rate equation in MATLAB for wetting layer we found the curves for electron density in wetting layer vs time. In this case we used the pumping currents, same as before, ranging from 1.3 j_{th} to 3.9 j_{th} . Variations of different curves for different pump currents are shown in the figure 4.3.

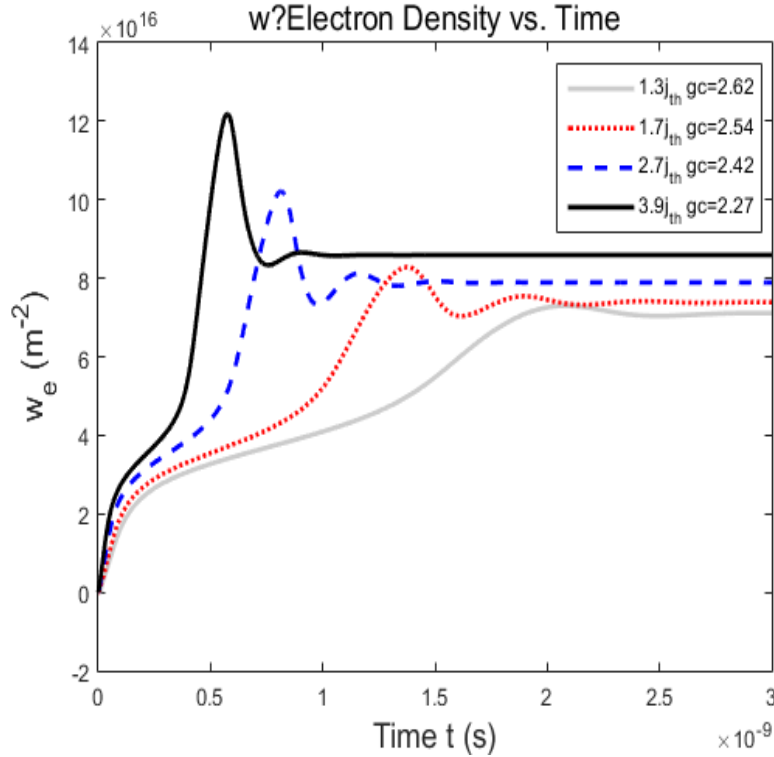


Figure 4.3: WL electron density vs time

Curves in this case somewhat follows the curves shown in electron and hole population density vs time in quantum dot layer. For higher pump currents steady state appears faster. In this situation, at first the curves increases rapidly. But after a certain point when it goes into steady state. Because of higher pump currents electron density in the wetting layer increases which causes the system to start emission earlier. Main difference in wetting layer electron density and quantum dot layer electron density is that a higher current results in a larger number of electrons in steady-state whereas in the QD this is not the case.

4.5 Wetting layer hole density vs Time:

Here we got the curve for hole density in the wetting layer vs time. This curve is somewhat similar to the curves in wetting layer electron density vs time. For different pumping currents, hole density in wetting layer varies which is shown in the figure

4.4. In this case also pumping current is used ranging from $1.3j_{th}$ to $3.9j_{th}$. j_{th} term is used for showing the threshold pumping current.

The figure is plot by putting WL hole density used as (m^{-2}) unit vs time described in seconds (s).

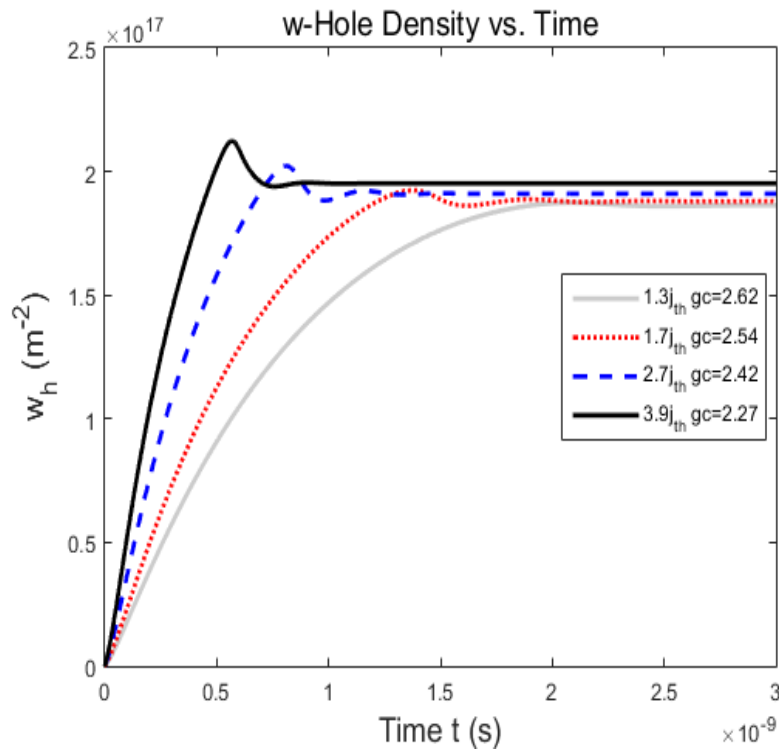


Figure 4.4: WL hole density vs time curves

For WL layer hole density, steady state appears faster for high pumping currents. As high pumping currents means large number of holes are being fed to the system which causes emission earlier.

The difference in WL hole density and QD layer hole density is that higher currents result in higher number of holes of wetting layer than QD layer.

We tried to simulate the system to steady state for different pump currents. Electron and hole density in WL are used as a function of pumping currents.

4.6 Electron density in wetting layer in steady state:

Electron density in WL in steady state vs pump current curve is shown in the figure 4.5.

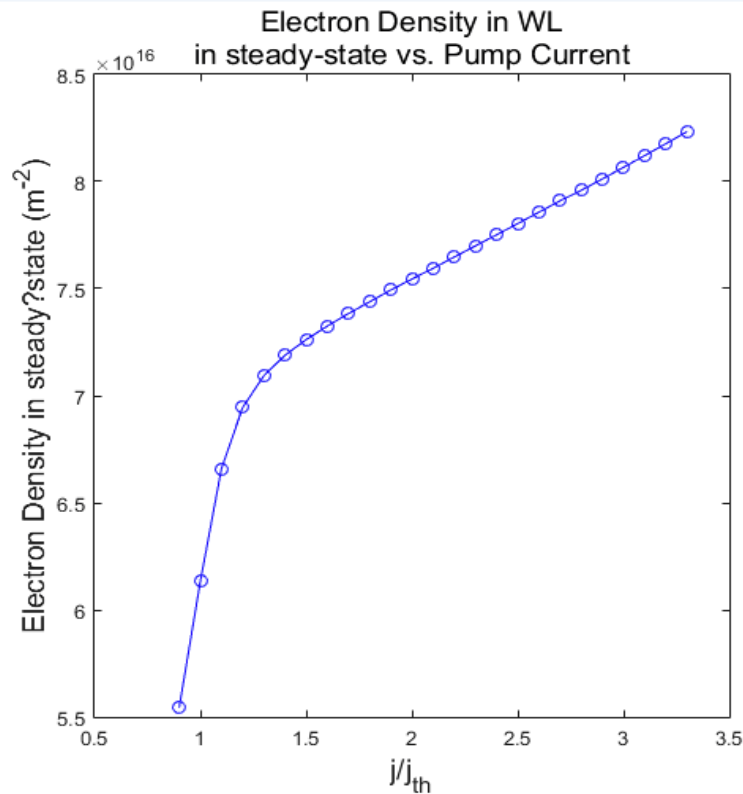


Figure 4.5: Electron density in WL in steady state vs pump current

From the figure 4.5, it is found that upto a certain threshold current, curve increases rapidly but after that it increases at a decrease rate. This happens because of the fact that a higher number of radiative transitions occur in QDs when pumping current is above the threshold current. As a result demand of electron from the WL increases. When the pump current is below the threshold current lasing effect is significantly reduced as the number of radiative transitions reduces. So, the demand for electron from the wetting layer decreases causing the curve to increase at a decreased rate. It is seen from the figure that before the threshold current there is a steep climb but above the threshold current the slope decreases.

4.7 Hole density in WL in steady state :

Hole density in wetting layer in steady state vs pump current, curve is shown in the figure 4.6.

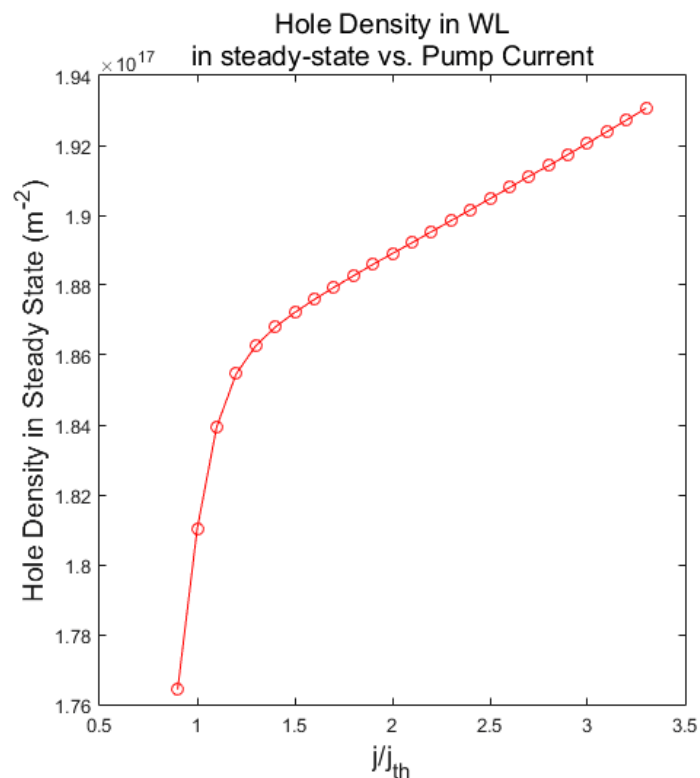


Figure 4.6: Hole density in WL in steady state vs pump current.

In this case also upto a threshold current there is a steep climb but after that threshold current the curve increases at a decrease rate. For higher currents, higher number of radiative transitions occur after the threshold current. As a result the demand for holes from WL in QD layer increases. Below the threshold current there is no lasing effect. So the demand for holes in QD layer from WL also decreases. The slope of the curve increases upto the threshold current then it decreases.

For this curve of electron and hole density in WL in steady state, a linear relation between densities in steady state and the currents is observed.

Chapter 5

Conclusion and future work

5.1 Conclusion

Here detailed analysis of quantum dot and quantum dot laser is done. Modeling of the quantum dot laser is also presented to get a proper idea of how quantum dot laser works and its various properties. Simulation of matlab codes of rate equations is done to get the proper general view of how the electrons and holes in quantum dot and wetting layer functions when the lasing effect starts and ends. The task that is accomplished can be summarized as follows-

- General idea of quantum dot and quantum dot laser is explained.
- Fabrication and different methods of production of quantum dot laser is explained in detail.
- Modeling of the quantum dot laser is explained.
- Finally the simulation of rate equations in Matlab to analyze different properties of electrons and holes in quantum dot and wetting layer before and after the lasing effect.

5.2 Future works

In the future, we have plans to elaborate on our present work on QDLs. To give more cleared picture of our future works, following list is provided-

- To carry out the small signal and large signal analysis of QDL using the RES model in MATLAB.
- To investigate the use of QDL in datacomm applications.
- To develop a more detailed and accurate model of QDL using experimental data of practical QDLs that have already been implemented.

References

- [1] Huiyun Liu*, Ting Wang, Qi Jiang, Richard Hogg, Frank Tutu1, Francesca Pozzi1 and Alwyn Seeds. Long-wavelength InAs/GaAs quantum-dot laser diode monolithically grown on Ge substrate. *Nature Photonics* 5, 416–419 (2011)
- [2] David Gready, Gadi Eisenstein, *Fellow, IEEE*, Vitalii Ivanov, Christian Gilfert, Florian Schnabel, Anna Rippien, Johann Peter Reithmaier, *Fellow, IEEE*, and Carsten Bornholdt. High Speed 1.55 μm InAs/InGaAlAs/InP Quantum Dot Lasers. *IEEE Photonics Technology Letters* (Volume: 26, Issue: 1, Jan.1, 2014)
- [3] Yating Wan, , Qiang Li, , Alan Y. Liu, , Weng W. Chow, Arthur C. Gossard, John E. Bowers, Evelyn L. Hu, and Kei May Lau, Sub-wavelength InAs quantum dot micro-disk lasers epitaxially grown on exact Si (001) substrates. *Appl. Phys. Lett.* **108**, 221101 (2016)
- [4] Alan Y. Liu, Chong Zhang, Justin Norman, Andrew Snyder, Dmitri Lubyshev, Joel M. Fastenau, Amy W. K. Liu, Arthur C. Gossard, and John E. Bowers. High performance continuous wave 1.3 μm quantum dot lasers on silicon. *Appl. Phys. Lett* 104, 041104 (2014)
- [5] Siming Chen, Wei Li, Jiang Wu, Qi Jiang, Mingchu Tang, Samuel Shutts, Stella N. Elliott, Angela Sobiesierski, Alwyn J. Seeds1, Ian Ross, Peter M. Snowton and Huiyun Liu. Electrically pumped continuous-wave III–V quantum dot lasers on silicon. *Nature Photonics* 10, 307–311 (2016).
- [6] Kristian Lund Jensen, Jesper Toft Kristensen, Jakob Rosenkrantz de Lasson. *Semiconductor Quantum Dots*.(2008)
- [7] Huizi Diwu, Betul Arda. *Quantum Dot Lasers*.
- [8] K. Lüdge et al., "Turn-on dynamics and modulation response in semiconductor quantum dot lasers," *Physical Review B* (published 17 July 2008).
- [9] R.V.N. Melnik and M. Willatzen, "Bandstructures of conical quantum dots with wetting layers," *Institute of Physics Publishing* (published 10 November 2003).
- [10] I. Vurgaftman and J. R. Meyer, "Band parameters for III-V compound semiconductors and their alloys," *J. Appl. Phys.*, Vol. 89, No. 11, 1 June 2001, pp. 5825-5826.

APPENDIX

A.MATLAB SIMULATION OF CARRIER DENSITY VS TIME:

```
%%%%%%%%%%%%%%%%%%%%%%%%%%%%%%%%%%%%%%%%%%%%%%%%%%%%%%%%%%%%%%%%%%%%%%%% Solving of coupled differential eqn. %%%%%%%%%%
%%%%%%%%%%%%%%%%%%%%%%%%%%%%%%%%%%%%%%%%%%%%%%%%%%%%%%%%%%%%%%%%%%%%%%%% Rate Equations for QD/WL System II %%%%%%%%%%
%%%%%%%%%%%%%%%%%%%%%%%%%%%%%%%%%%%%%%%%%%%%%%%%%%%%%%%%%%%%%%%%%%%%%%%%
close all
clear all
clc
format long e
%%% User input ? simulation time %%%
sim_time = input('Simulation time in nanoseconds: ');
%%%

%%% Universal constants:
e_0 = 1.602e-19; % Elementary charge.
W = 1.3*(1e-9)^(-1); % Einstein coefficient

% %%% Quantum System Parameters:
kappa = 0.12*(1e-12)^(-1); % Total cavity loss.
Gamma = 0.0011; % Optical confinement factor.
beta = 5e-6; % Probability that photon contributes to laser mode.

%%% Macro System Parameters:
A = 4e-9; % The WL normalisation area.
N_QD = 1e14; % No of QD pr. area substrate
N_WL = 2e17; % No of QD pr. area substrate
j_th = 1.799*10^(10)*e_0*10^(4)*(10^(-12))^(-1); % Thredshold dens.
current.
t_0 = 2.49e-9; % Translation constant of pulse top.
eta = 90; % Power in current pulse.

%%% Initial conditions:
n_init = [0, 0, 0, 0, 0]; % Set initial no. of electrons.

% %%% Colors and styles Photon Plot
% colr = [[0.87059 0.4902 0];...
% 1 0 0 ;...
% 0 0 1;...
% 0.8 0.8 0.8;...
% 0.8 0.8 0.8;...
% 0 0 0];
%
% stl = char('?.','?','??','?.','?','?');
% linewidth = 2;
% %%%

%%% Colors and styles Population Plots
colr = [0.8 0.8 0.8;...
1 0 0 ;...
```

```

0 0 1;...
0 0 0];

stl = char('-', ':', '--', '-');
linewidth = 2;
%%%

%%% Numeric parameters:
delta_t = 1e-15; % Time step size.
no_of_steps = ceil(sim_time*1e-9/delta_t); % No. of time steps.

display(['Simulation Time: ', num2str(sim_time), ' ns']);
display(['Number of steps: ', num2str(no_of_steps)]);
display(['Time step: ', num2str(delta_t), ' s']);

current_values_loop = [ 1.3, 1.7, 2.7, 3.9 ];
current_graph_color = char('c--', 'r-', 'b--', 'g--', 'm-', 'k-');
current_graph_legend = char([num2str(current_values_loop(1)), 'j_{th}'], ...
[num2str(current_values_loop(2)), 'j_{th}'], ...
[num2str(current_values_loop(3)), 'j_{th}'], ...
[num2str(current_values_loop(4)), 'j_{th}']);
% [num2str(current_values_loop(5)), 'j_{th}'], ...
% [num2str(current_values_loop(6)), 'j_{th}']);

gc = zeros(1, length(current_values_loop));
for g = 1:length(current_values_loop)
j_0 = current_values_loop(g)*j_th; % Current density through system [A/m^2]

gc_pre = 1; % Previous g_c
gc(g) = 2.5; % Current g_c

%%%%%%%% Self-consistent g_c structure: %%%%%%%%%
while abs(gc_pre-gc(g))/gc_pre > 0.01 %Tolerance on the true gc?value

%%% Initialisation:
t_values = zeros(1, no_of_steps); % Preallocating: Time. values.
n = zeros(no_of_steps, 5); % Preallocating: Func. values.
j = zeros(1, no_of_steps); % Preallocating: current dens. values.
t = 0; % Initial time.

n_run = n_init; % Initial no. of electrons.

S_in_e = zeros(1, no_of_steps);
S_in_h = zeros(1, no_of_steps);
S_out_e = zeros(1, no_of_steps);
S_out_h = zeros(1, no_of_steps);

for k = 1:no_of_steps
j(k) = j_0*exp(-((t-t_0)/(2.5e-9))^eta); %Current density.

%%% Radiative scattering rates:
R_ind = W*A*(n_run(1)+n_run(2)-N_QD)*n_run(5);
R_sp = (W/N_QD)*n_run(1)*n_run(2);
R_WL_sp = (W/N_WL)*n_run(3)*n_run(4);

%%% Scale factors for fits converting units to SI
sc = 10^(-15);
vertsc = 10^(12);
%%%

```

```

% S_in_e:
F_in_e = 0.715+0.6*gc(g)-0.19*gc(g)^2;
B_in_e = -6.9 + 40.5*gc(g)-11*gc(g)^2;
A_in_e = 0.0116;

%S_in_h:
A_in_h = 8 + 0.228*gc(g);
B_in_h = 0.096 - 0.0095*gc(g);
C_in_h = 171;

%S_out_h:
F_out_h = 0.2823 + 0.0201*gc(g);
D_out_h = -0.9 - 3*gc(g);

%S_out_e:
B_out_e = 963 - 153*gc(g);
C_out_e = 12.4 - 5.35*gc(g) + 0.718*gc(g)^2;
A_out_e = 0.1154;
%%%
%%%%%% The non?radiative scattering rates:
%%%% S_in_e
if n_run(3) <= 0
S_in_e(k) = 0;
else

argument1 = (38-n_run(3)*sc)/B_in_e;
argument2 = (38-n_run(3)*sc)/5.4;

if argument2 > 709

S_in_e(k) = (A_in_e*...
exp(-2*(n_run(3)*sc-124.5)^2/29.6^2))*vertsc;
%The 2nd factor in the first term becomes zero.

elseif argument1 > 709

S_in_e(k) = ...
(F_in_e*(1/(1 + exp((38-n_run(3)*sc)/5.4))))+...
A_in_e*exp(-2*(n_run(3)*sc-124.5)^2/29.6^2))...
*vertsc; %The 3rd factor in the first term has
%been set to one to avoid divergence.
else % No divergence
S_in_e(k) = ...
(F_in_e*(1/(1 + exp((38-n_run(3)*sc)/5.4))))*...
(exp((38-n_run(3)*sc)/B_in_e)/...
(1 + exp((38-n_run(3)*sc)/B_in_e)))+...
A_in_e*exp(-2*(n_run(3)*sc-124.5)^2/29.6^2))...
*vertsc;
end

end
%%%
%%%% S_in_h
S_in_h(k) = tanh(B_in_h*n_run(4)*sc)*A_in_h*...
exp(-2*(n_run(4)*sc-182)^2/C_in_h^2)*vertsc...
/(C_in_h*sqrt(pi/2));
%%%
%%%% S_out_h

```

```

% Function value in the point from where linear extrapolation is
%needed:
Const_S_out_h = (F_out_h*(1-exp(-(1.2e15*sc-1.2)/1.7))^(0.7)*...
exp(-(1.2e15*sc)^2/18854)+...
exp(-(1.2e15*sc-D_out_h)/26.4));

if n_run(4) < 1.2e15
S_out_h(k) = Const_S_out_h*vertsc*n_run(4)/(1.2)*sc;
else
S_out_h(k) = (F_out_h*(1-exp(-(n_run(4)*sc-1.2)/1.7))^(0.7)*...
exp(-(n_run(4)*sc)^2/18854)+...
exp(-(n_run(4)*sc-D_out_h)/26.4))*vertsc;
end
%%%%
%% S_out_e
% Function value in the point from where linear extrapolation is
%needed:
Const_S_out_e = ((1-exp((1-0.1e16*sc)/2))^(0.9)*exp(-0.1e16...
*sc)^2/B_out_e)+exp((1.73-0.1e16*sc)/C_out_e)+...
A_out_e*exp(-(0.1e16*sc-27.5)^2/137.8));

if n_run(3) < 0.1e16
S_out_e(k) = Const_S_out_e*vertsc*n_run(3)/(1)*sc;
else
S_out_e(k) = ((1-exp((1-n_run(3)*sc)/2))^(0.9)*exp(-(n_run(3)...
*sc)^2/B_out_e)+exp((1.73-n_run(3)*sc)/C_out_e)+...
A_out_e*exp(-(n_run(3)*sc-27.5)^2/137.8))*vertsc;
end
%%%%

tau_e = (S_in_e(k)+S_out_e(k))^(-1); % Scattering times electrons.
tau_h = (S_in_h(k)+S_out_h(k))^(-1); % Scattering times holes.

t_values(k) = t; % Save time in matrix
n(k,:) = n_run; % Save no. of carriers at all levels at time t.

% Differential eqn. system or Rate eqn. system (RES):
dn_dt = ...
[-1/tau_e*n_run(1)+S_in_e(k)*N_QD-R_ind-R_sp,...
-1/tau_h*n_run(2)+S_in_h(k)*N_QD-R_ind-R_sp,...
j(k)/e_0+n_run(1)/tau_e*N_WL/N_QD-S_in_e(k)*N_WL-R_WL_sp, ...
j(k)/e_0+n_run(2)/tau_h*N_WL/N_QD-S_in_h(k)*N_WL-R_WL_sp, ...
-2*kappa*n_run(5)+Gamma*R_ind+beta*R_sp];

t = t + delta_t; % Time stepped.
n_run = n_run + dn_dt*delta_t; %No. of carriers stepped at all levels.
end

gc_pre = gc(g);
gc(g) = n(4e6,4)/n(4e6,3);

end % END Self?consistent g_c structure
%% Plot development:
figure(11)
plot(t_values(1:3e6),n(1:3e6,1),'LineStyle',stl(g,:), 'Color',[colr(g,:)],...
'LineWidth',linewidth);
title('n-Electron Density vs. Time','FontWeight','demi','FontSize',14,...
'FontName','Arial');
legend([current_graph_legend(1,:), ' gc=', num2str(roundn(gc(1),-2))],...

```

```

[current_graph_legend(2,:), ' gc=', num2str(roundn(gc(2),-2))], ...
[current_graph_legend(3,:), ' gc=', num2str(roundn(gc(3),-2))], ...
[current_graph_legend(4,:), ' gc=', num2str(roundn(gc(4),-2))], ...
'Location', 'Best')
xlabel('Time t (s)', 'FontSize', 14, 'FontName', 'Arial')
ylabel('n_{e} (m^{-2})', 'FontSize', 14, 'FontName', 'Arial')
hold on

figure(8)

plot(t_values(1:3e6), n(1:3e6, 2), 'LineStyle', stl(g,:), 'Color', [colr(g,:)] ...
, 'LineWidth', linewidth);
title('n-Hole Density vs. Time', 'FontWeight', 'demi', 'FontSize', 14, ...
'FontName', 'Arial');
legend([current_graph_legend(1,:), ' gc=', num2str(roundn(gc(1),-2))], ...
[current_graph_legend(2,:), ' gc=', num2str(roundn(gc(2),-2))], ...
[current_graph_legend(3,:), ' gc=', num2str(roundn(gc(3),-2))], ...
[current_graph_legend(4,:), ' gc=', num2str(roundn(gc(4),-2))], ...
'Location', 'Best')
xlabel('Time t (s)', 'FontSize', 14, 'FontName', 'Arial')
ylabel('n_{h} (m^{-2})', 'FontSize', 14, 'FontName', 'Arial')
hold on

figure(9)

plot(t_values(1:3e6), n(1:3e6, 3), 'LineStyle', stl(g,:), 'Color', [colr(g,:)] ...
, 'LineWidth', linewidth);
title('w?Electron Density vs. Time', 'FontWeight', 'demi', 'FontSize', 14, ...
'FontName', 'Arial');
legend([current_graph_legend(1,:), ' gc=', num2str(roundn(gc(1),-2))], ...
[current_graph_legend(2,:), ' gc=', num2str(roundn(gc(2),-2))], ...
[current_graph_legend(3,:), ' gc=', num2str(roundn(gc(3),-2))], ...
[current_graph_legend(4,:), ' gc=', num2str(roundn(gc(4),-2))], ...
'Location', 'Best')
xlabel('Time t (s)', 'FontSize', 14, 'FontName', 'Arial')
ylabel('w_{e} (m^{-2})', 'FontSize', 14, 'FontName', 'Arial')
hold on

figure(10)

plot(t_values(1:3e6), n(1:3e6, 4), 'LineStyle', stl(g,:), 'Color', [colr(g,:)] ...
, 'LineWidth', linewidth);
title('w-Hole Density vs. Time', 'FontWeight', 'demi', 'FontSize', 14, ...
'FontName', 'Arial');
legend([current_graph_legend(1,:), ' gc=', num2str(roundn(gc(1),-2))], ...
[current_graph_legend(2,:), ' gc=', num2str(roundn(gc(2),-2))], ...
[current_graph_legend(3,:), ' gc=', num2str(roundn(gc(3),-2))], ...
[current_graph_legend(4,:), ' gc=', num2str(roundn(gc(4),-2))], ...
'Location', 'Best')
xlabel('Time t (s)', 'FontSize', 14, 'FontName', 'Arial')
ylabel('w_{h} (m^{-2})', 'FontSize', 14, 'FontName', 'Arial')
hold on

% figure(1)
%
plot(t_values(1:3e6), n(1:3e6, 5), 'LineStyle', stl(g,:), 'Color', [colr(g,:)] ...
, 'LineWidth', linewidth);
%
%
% title('Photon Density vs. Time', 'FontWeight', 'demi', 'FontSize', 14, ...
% 'FontName', 'Arial');

```

```

% legend([current_graph_legend(1,:), ' gc=', num2str(roundn(gc(1), ?2))], ...
% [current_graph_legend(2,:), ' gc=', num2str(roundn(gc(2), ?2))], ...
% [current_graph_legend(3,:), ' gc=', num2str(roundn(gc(3), ?2))], ...
% [current_graph_legend(4,:), ' gc=', num2str(roundn(gc(4), ?2))], ...
% [current_graph_legend(5,:), ' gc=', num2str(roundn(gc(5), ?2))], ...
% [current_graph_legend(6,:), ' gc=', num2str(roundn(gc(6), ?2))], ...
% 'Location', 'Best')
% xlabel('Time t (s)', 'FontSize', 14, 'FontName', 'Arial')
% ylabel('Photon Density n_{ph}
(m^{?2})', 'FontSize', 14, 'FontName', 'Arial')
% hold on

end % end of for loop ? currents
hold off

```

B.MATLAB SIMULATION CODE FOR CARRIER DENSITY AT STEADY STATE:

```

%%%%%%%%%%%%%%%%%%%%%%%%%%%%%%%%%%%%%%%%%%%%%%%%%%%%%%%%%%%%%%%%%%%%%%%% Solving of coupled differential eqn. %%%%%%%%%
%%%%%%%%%%%%%%%%%%%%%%%%%%%%%%%%%%%%%%%%%%%%%%%%%%%%%%%%%%%%%%%%%%%%%%%% Rate Equations for QD/WL System II %%%%%%%%%
%%%%%%%%%%%%%%%%%%%%%%%%%%%%%%%%%%%%%%%%%%%%%%%%%%%%%%%%%%%%%%%%%%%%%%%%
close all
clear all
clc
format long e

%%% User input ? simulation time %%%
sim_time = input('steady-state time: ');
%%%

%%% Universal constants:
e_0 = 1.602e-19; % Elementary charge.
W = 1.3*(1e-9)^(-1); % Einstein coefficient

% %%% Quantum System Parameters:
kappa = 0.12*(1e-12)^(-1); % Total cavity loss.
Gamma = 0.0011; % Optical confinement factor.
beta = 5e-6; % Probability that photon contributes to laser mode.

%%% Macro System Parameters:
A = 4e-9; % The WL normalisation area.
N_QD = 1e14; % No of QD pr. area substrate
N_WL = 2e17; % No of QD pr. area substrate
j_th = 1.799*10^(10)*e_0*10^(4)*(10^(-12))^(-1); % Thredshold dens.
current.
t_0 = 2.49e-9; % Translation constant of pulse top.
eta = 90; % Power in current pulse.

%%% Initial conditions:
n_init = [0, 0, 0, 0, 0]; % Set initial no. of electrons.

%%% Numeric parameters:

```



```

delta_t = 1e-15; % Time step size.
no_of_steps = ceil(sim_time*1e-9/delta_t); % No. of time steps.

display(['Simulation Time: ', num2str(sim_time), ' ns']);
display(['Number of steps: ', num2str(no_of_steps)]);
display(['Time step: ', num2str(delta_t), ' s']);

current_values_loop = [ 0.9:0.1:3.3 ]; %Currents to be included

% g_c values calc. using the self-consistent g_c script:
gc =
[3.193902007048897e+00,2.951302464725806e+00,2.761449643887285e+00,...
2.669448228848847e+00,2.624804722360130e+00,2.597285940973115e+00,...
2.577024874233112e+00,2.559820943187693e+00,2.544401259010151e+00,...
2.530232358304601e+00,2.519586982551862e+00,2.504480683356124e+00,...
2.489450076239233e+00,2.478964457684705e+00,2.466965271820845e+00,...
2.455176553965381e+00,2.443570075276678e+00,2.432124203391949e+00,...
2.420823785821585e+00,2.403763005747533e+00,2.391424707627967e+00,...
2.379052916937061e+00,2.366631640442151e+00,2.354145211603275e+00,...
2.341577868643550e+00,];

Current_population = zeros(length(current_values_loop),3);

for g = 1:length(current_values_loop)
j_0 = current_values_loop(g)*j_th; % Current density through system
% [A/m^2]

%%% Initialisation:
t_values = zeros(1,no_of_steps); % Preallocating: Time. values.
n = zeros(no_of_steps,5); % Preallocating: Func. values.
j = zeros(1,no_of_steps); % Preallocating: current dens. values.
t = 0; % Initial time.

n_run = n_init; % Initial no. of electrons.

S_in_e = zeros(1,no_of_steps);
S_in_h = zeros(1,no_of_steps);
S_out_e = zeros(1,no_of_steps);
S_out_h = zeros(1,no_of_steps);
for k = 1:no_of_steps
j(k) = j_0*exp(-((t-t_0)/(2.5e-9))^eta); %Current density.

%%% Radiative scattering rates:
R_ind = W*A*(n_run(1)+n_run(2)-N_QD)*n_run(5);
R_sp = (W/N_QD)*n_run(1)*n_run(2);
R_WL_sp = (W/N_WL)*n_run(3)*n_run(4);

%%% Scale factors for fits converting units to SI
sc = 10^(-15);
vertsc = 10^(12);
%%%

% S_in_e:
F_in_e = 0.715+0.6*gc(g)-0.19*gc(g)^2;
B_in_e = -6.9 + 40.5*gc(g)-11*gc(g)^2;
A_in_e = 0.0116;

%S_in_h:
A_in_h = 8 + 0.228*gc(g);

```

```

B_in_h = 0.096 - 0.0095*gc(g);
C_in_h = 171;

%S_out_h:
F_out_h = 0.2823 + 0.0201*gc(g);
D_out_h = -0.9 - 3*gc(g);

%S_out_e:
B_out_e = 963 - 153*gc(g);
C_out_e = 12.4 - 5.35*gc(g) + 0.718*gc(g)^2;
A_out_e = 0.1154;
%%%

%%%%%%%% The non-radiative scattering rates:
%%% S_in_e
if n_run(3) <= 0
S_in_e(k) = 0;
else

argument1 = (38-n_run(3)*sc)/B_in_e;
argument2 = (38-n_run(3)*sc)/5.4;

if argument2 > 709

S_in_e(k) = (A_in_e*...
exp(-2*(n_run(3)*sc-124.5)^2/29.6^2))*vertsc;
%The 2nd factor in the first term becomes zero.

elseif argument1 > 709

S_in_e(k) = ...
(F_in_e*(1/(1 + exp((38-n_run(3)*sc)/5.4))))+...
A_in_e*exp(-2*(n_run(3)*sc-124.5)^2/29.6^2))*...
*vertsc; %The 3rd factor in the first term has
%been set to one to avoid divergence.
else % No divergence
S_in_e(k) = ...
(F_in_e*(1/(1 + exp((38-n_run(3)*sc)/5.4)))*...
(exp((38-n_run(3)*sc)/B_in_e)/...
(1 + exp((38-n_run(3)*sc)/B_in_e))))+...
A_in_e*exp(-2*(n_run(3)*sc-124.5)^2/29.6^2))*...
*vertsc;
end

end

%%%
%%% S_in_h
S_in_h(k) = tanh(B_in_h*n_run(4)*sc)*A_in_h*...
exp(-2*(n_run(4)*sc-182)^2/C_in_h^2)*vertsc...
/(C_in_h*sqrt(pi/2));
%%%
%%% S_out_h

% Function value in the point from where linear extrapolation is
% needed:
Const_S_out_h = (F_out_h*(1-exp(-(1.2e15*sc-1.2)/1.7))^(0.7)*...
exp(-(1.2e15*sc)^2/18854)+...
exp(-(1.2e15*sc-D_out_h)/26.4));

```

```

if n_run(4) < 1.2e15
S_out_h(k) = Const_S_out_h*vertsc*n_run(4)/(1.2)*sc;
else
S_out_h(k) = (F_out_h*(1-exp(-(n_run(4)*sc-1.2)/1.7))^(0.7)*...
exp(-(n_run(4)*sc)^2/18854)+...
exp(-(n_run(4)*sc-D_out_h)/26.4))*vertsc;
end
%%%%
%% S_out_e

% Function value in the point from where linear extrapolation is
% needed:
Const_S_out_e = ((1-exp((1-0.1e16*sc)/2))^(0.9)*exp(-(0.1e16...
*sc)^2/B_out_e)+exp((1.73-0.1e16*sc)/C_out_e)+...
A_out_e*exp(-(0.1e16*sc-27.5)^2/137.8));

if n_run(3) < 0.1e16
S_out_e(k) = Const_S_out_e*vertsc*n_run(3)/(1)*sc;
else
S_out_e(k) = ((1-exp((1-n_run(3)*sc)/2))^(0.9)*exp(-(n_run(3)...
*sc)^2/B_out_e)+exp((1.73-n_run(3)*sc)/C_out_e)+...
A_out_e*exp(-(n_run(3)*sc-27.5)^2/137.8))*vertsc;
end
%%%%

tau_e = (S_in_e(k)+S_out_e(k))^(-1); % Scattering times electrons.
tau_h = (S_in_h(k)+S_out_h(k))^(-1); % Scattering times holes.

t_values(k) = t; % Save time in matrix
n(k,:) = n_run; % Save no. of carriers at all levels at time t.

% Differential eqn. system or Rate eqn. system (RES):
dn_dt = ...
[-1/tau_e*n_run(1)+S_in_e(k)*N_QD-R_ind-R_sp,...
-1/tau_h*n_run(2)+S_in_h(k)*N_QD-R_ind-R_sp,...
j(k)/e_0+n_run(1)/tau_e*N_WL/N_QD-S_in_e(k)*N_WL-R_WL_sp, ...
j(k)/e_0+n_run(2)/tau_h*N_WL/N_QD-S_in_h(k)*N_WL-R_WL_sp, ...
-2*kappa*n_run(5)+Gamma*R_ind+beta*R_sp];

t = t + delta_t; % Time stepped.

if k == no_of_steps
clc
Current_population(g,1) = j(k)/j_th;
Current_population(g,2) = n_run(3);
Current_population(g,3) = n_run(4);
disp([num2str(g/length(Current_population(:,1))*100), '%']);
end

n_run = n_run + dn_dt*delta_t; % No. of carriers stepped at all levels.
end

end % end of for loop ? currents

%% Plots the results:
scrsz = get(0, 'ScreenSize');

```

```

figure1 = figure('Position',[scrsz(3)/4 scrsz(4)/4 1200 scrsz(4)/2]);

subplot(1,2,1,'Parent',figure1)
plot(Current_population(:,1),Current_population(:,2),'o-b')
title(...
['Electron Density in WL',sprintf('\n'),...
'in steady-state vs. Pump Current'],'FontWeight','demi','FontSize',...
14,'FontName','Arial');
xlabel('j/j_{th}','FontSize',14,'FontName','Arial')
ylabel('Electron Density in steady?state (m^{-2})','FontSize',14,...
'FontName','Arial')
% xlim([min(Current_population(:,1))*0.9 ...
%max(Current_population(:,1))*1.1])
% ylim([min(Current_population(:,2))*0.995 ...
% max(Current_population(:,2))*1.005])
subplot(1,2,2,'Parent',figure1)
plot(Current_population(:,1),Current_population(:,3),'o-r')
title(...
['Hole Density in WL',sprintf('\n'),...
'in steady-state vs. Pump Current'],'FontWeight','demi','FontSize',...
14,'FontName','Arial');

xlabel('j/j_{th}','FontSize',14,'FontName','Arial')
ylabel('Hole Density in Steady State (m^{-2})','FontSize',14,...
'FontName','Arial')
% xlim([min(Current_population(:,1))*0.9 ...
% max(Current_population(:,1))*1.1])
% ylim([min(Current_population(:,3))*0.999 ...
% max(Current_population(:,3))*1.001])

```